JACS
JOURNAL OF THE AMERICAN CHEMICAL SOCIETY
Article
pubs.acs.org/JACS

Mechanical Bonds and Topological Effects in Radical Dimer Stabilization

Marco Frasconi,[†] Takashi Kikuchi,[†] Dennis Cao,[†] Yilei Wu,[†,‡] Wei-Guang Liu,[§] Scott M. Dyar,[†,‡] Gokhan Barin,[†] Amy A. Sarjeant,[†] Charlotte L. Stern,[†] Raanan Carmieli,[†,‡] Cheng Wang,[†,∥] Michael R. Wasielewski,[†,‡] William A. Goddard III,[§,⊥] and J. Fraser Stoddart*[,†]

[†]Department of Chemistry, Northwestern University, 2145 Sheridan Road, Evanston, Illinois 60208, United States

[‡]Argonne-Northwestern Solar Energy Research (ANSER) Center, Northwestern University, 2145 Sheridan Road, Evanston, Illinois 60208, United States

[§]Materials and Process Simulation Center, California Institute of Technology, Pasadena, California 91125, United States

[∥]College of Chemistry and Molecular Science, Wuhan University, Wuhan, Hubei Province 430072, People's Republic of China

[⊥]NanoCentury KAIST Institute and Graduate School of EEWS (WCU), Korea Advanced Institute of Science and Technology (KAIST), 373-1 Guseong Dong, Yuseong Gu, Daejeon 305-701, Republic of Korea

Supporting Information

ABSTRACT: While mechanical bonding stabilizes tetrathiafulvalene (TTF) radical dimers, the question arises: what role does topology play in catenanes containing TTF units? Here, we report how topology, together with mechanical bonding, in isomeric [3]- and doubly interlocked [2]catenanes controls the formation of TTF radical dimers within their structural frameworks, including a ring-in-ring complex (formed between an organoplatinum square and a {2+2} macrocyclic polyether containing two 1,5-dioxynaphthalene (DNP) and two TTF units) that is topologically isomeric with the doubly interlocked [2]catenane. The separate TTF units in the two {1+1} macrocycles (each containing also one DNP unit) of the isomeric [3]catenane exhibit slightly different redox properties compared with those in the {2+2} macrocycle present in the [2]catenane, while comparison with its topological isomer reveals substantially different redox behavior. Although the stabilities of the mixed-valence $(TTF_2)^{\bullet+}$ dimers are similar in the two catenanes, the radical cationic $(TTF^{\bullet+})_2$ dimer in the [2]catenane occurs only fleetingly compared with its prominent existence in the [3]catenane, while both dimers are absent altogether in the ring-in-ring complex. The electrochemical behavior of these three radically configurable isomers demonstrates that a fundamental relationship exists between topology and redox properties.

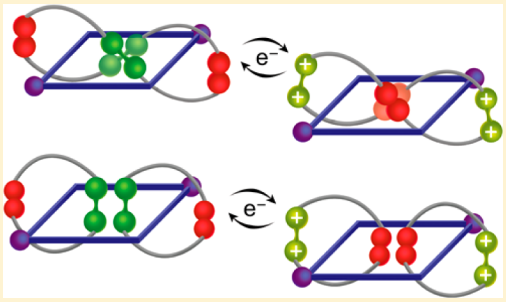

1. INTRODUCTION

Living systems are characterized by intricate interactions between wide collections of very different naturally occurring macromolecules which lead to the formation of bioconjugates that preside over a diverse range of biological functions. Yet, even within any given family of macromolecules, take the proteins, for example, the propensity[1,2] of their components, namely, the polypeptide chains, to not only fold but also become deeply knotted[3] suggests that topology plays a crucial role in establishing their functions, as well as their evolution. Elucidating the role that topology plays in biological systems poses a considerable challenge to the contemporary scientific community. The discovery that, in addition to conferring[4] stability upon bioactive cysteine knot proteins, the knotted topology leads to a highly specific redox-controlled folding mechanism involving a feature that has yet to be identified and appears to mediate and participate in the proteins' biological functions marks a significant realization at a fundamental level in science.

The interest shown by chemists in topology appears to have preceded that of the biologists and seems to have been aroused by mathematicians,[5,6] no more so than by Peter Guthrie Tait,[5] who not only began tabulating knots by hand in the 1870s but also drew attention to their chiralities, introducing also the term amphichiral[7] to describe achiral knots. Since Frisch and Wasserman[8] coined the term "chemical topology"[9−11] in 1961 and Walba[12] published his seminal review on topological stereochemistry in 1985, chemists[9,10] have devised a number of synthetic protocols, none more efficient than those[13−18] that depend on templation, that lead to the production of topologically nontrivial molecules, which can be either (i) achiral (amphichiral), (ii) conditionally chiral, or (iii) unconditionally chiral. The molecules, which are also characterized[19] by mechanical interlocking, include the catenanes,[20] trefoil[21] and pentafoil[22] knots, Solomon links,[23] and Borromean rings.[24]

Received: May 9, 2014
Published: July 10, 2014

dx.doi.org/10.1021/ja504662a | J. Am. Chem. Soc. 2014, 136, 11011−11026

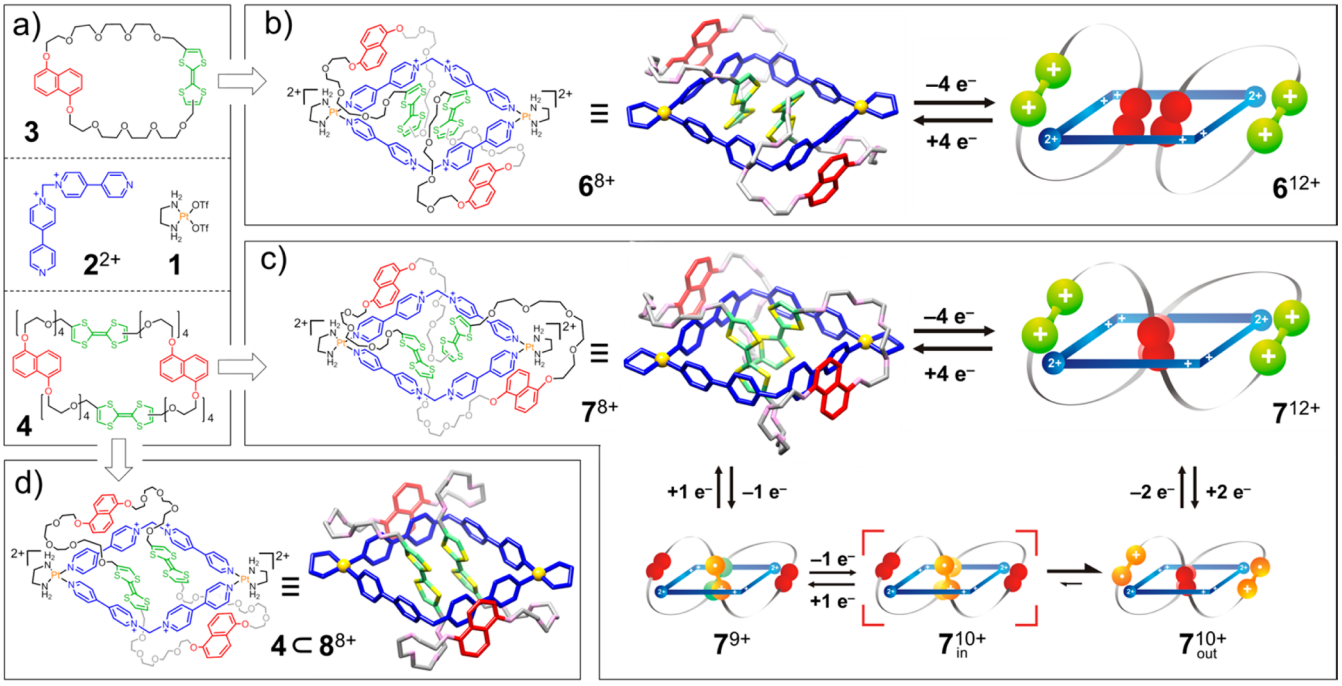

Figure 1. (a) The retrosynthesis of the [3]catenane $\mathbf{6}^{8+}$, the molecular Solomon link $\mathbf{7}^{8+}$, and the ring-in-ring complex $\mathbf{4}\subset\mathbf{8}^{8+}$. The structural formulas (left), the solid-state structures (center), and graphical representations (right) of the redox switching of (b) $\mathbf{6}^{8+}$ and (c) $\mathbf{7}^{8+}$, along with the redox switching mechanism (bottom) exhibited by the molecular Solomon link. Only one enantiomer of the molecular Solomon link, which has topological chirality, is shown. (d) The structural formula (left) and the perspective view of the solid-state superstructure (right) of $\mathbf{4}\subset\mathbf{8}^{8+}$. Hydrogen atoms, MeCN solvent molecules, and PF_6^- counterions are omitted for the sake of clarity.

Apart from their aesthetic charm, which is part of the motivation for chemists to design and create topologically complex molecules, the topology of a molecule, along with its geometry, has been identified[25] as being able to influence the properties and functions of molecular compounds. Despite the implication that the physicochemical and functional properties of compounds can be influenced by topology, this aspect of stereochemistry has not been explored in depth yet by chemists. By contrast, the practical importance of topology has been demonstrated in the field of materials science, where the presence of microscopic knots and links disclose unusual properties and functions to polymers[26] and chiral nematic colloids[27] based on their topology. Here, we explore the concept of topological effects at the molecular level through the experimental and theoretical investigation of the radical recognition processes of tetrathiafulvalene (TTF) within the molecular frameworks of three isomers, namely (1) a doubly interlocked [2]catenane, that is, a molecular Solomon link, (2) a [3]catenane, and (3) a ring-in-ring complex. TTF has attracted much attention in recent years[28] on account of its unique electronic properties[29] and has been used to prepare a number[30] of artificial molecular switches[31] (AMSs) by virtue of its π-donating ability and the (electro)chemical switchability of its electronic states. The strong electronic coupling that exists between the radical cation ($TTF^{\bullet+}$) and neutral parent (TTF^0), which are known to form upon one electron oxidation, leads to π-electron delocalization, also referred to as mixed-valence dimerization.[32] The formation of this mixed-valence dimer $(TTF_2)^{\bullet+}$, in conjunction with the radical cationic dimer $(TTF^{\bullet+})_2$, has been probed[33] previously in detail in the mechanically interlocked frameworks of [3]catenanes.

Herein, we describe (1) the syntheses, from the constituents (Figure 1a), namely, the ethylenediamine-chelated Pt(II) complex $\mathbf{1}^{2+}$ and the bent bidentate dicationic ligand $\mathbf{2}^{2+}$ of an organoplatinum square $\mathbf{8}^{8+}$ and from the {1+1} and {2+2} macrocyclic polyethers, that is, **3** and **4**, that contain, respectively, two and four alternating TTF and 1,5-dioxynaphthalene (DNP) units, of the [3]catenane $\mathbf{6}^{8+}$ (Figure 1b), the molecular Solomon link $\mathbf{7}^{8+}$ (Figure 1c), and the ring-in-ring complex $\mathbf{4}\subset\mathbf{8}^{8+}$ (Figure 1d), before carrying out (2) a detailed mechanistic investigation using ^{1}H NMR spectroscopy and single crystal X-ray crystallography of the redox-active behavior displayed by the two TTF units located in the middle of the framework of the molecular Solomon link $\mathbf{7}^{8+}$. As a result of a comparison of the radical chemistry of $\mathbf{7}^{8+}$ with that of the topologically isomeric ring-in-ring complex $\mathbf{4}\subset\mathbf{8}^{8+}$, as well as that of the mechanically distinguishable, constitutionally isomeric [3]catenane $\mathbf{6}^{8+}$, we have been able to elucidate an exquisite interplay between the mechanical bonds and topological effects on the molecular properties. By employing UV−vis−NIR and EPR spectroscopies, in addition to detailed electrochemical investigations in solution, we have investigated (3) the relative translational motions of the mechanically interlocked components within the molecular Solomon link upon successive oxidation of its TTF units; this process involves the movement of the crown ether within the molecular Solomon link, reminiscent of *reptation*,[34] to reach a stable geometry in which both DNP units are located inside the structural framework of the organoplatinum square. Of particular interest is the redox activation of a mixed-valence dimer $(TTF_2)^{\bullet+}$ between the two TTF units after a one-electron oxidation within the restricted inner space of the square. This mixed-valence dimer is stabilized by virtue of the mechanical bonds present in the molecular Solomon link $\mathbf{7}^{8+}$. Comparison of the TTF radical species in $\mathbf{7}^{8+}$ with those obtained in its constitutional isomer, the [3]catenane $\mathbf{6}^{8+}$,

dx.doi.org/10.1021/ja504662a | J. Am. Chem. Soc. 2014, 136, 11011−11026

Scheme 1. Synthesis of the Two [3]Catenanes 6·8PF$_6$ and 9·8PF$_6$,[a] the Two Molecular Solomon Links 7·8PF$_6$ and 10·8PF$_6$,[b] and the Organoplatinum Square 8·8PF$_6$[c]

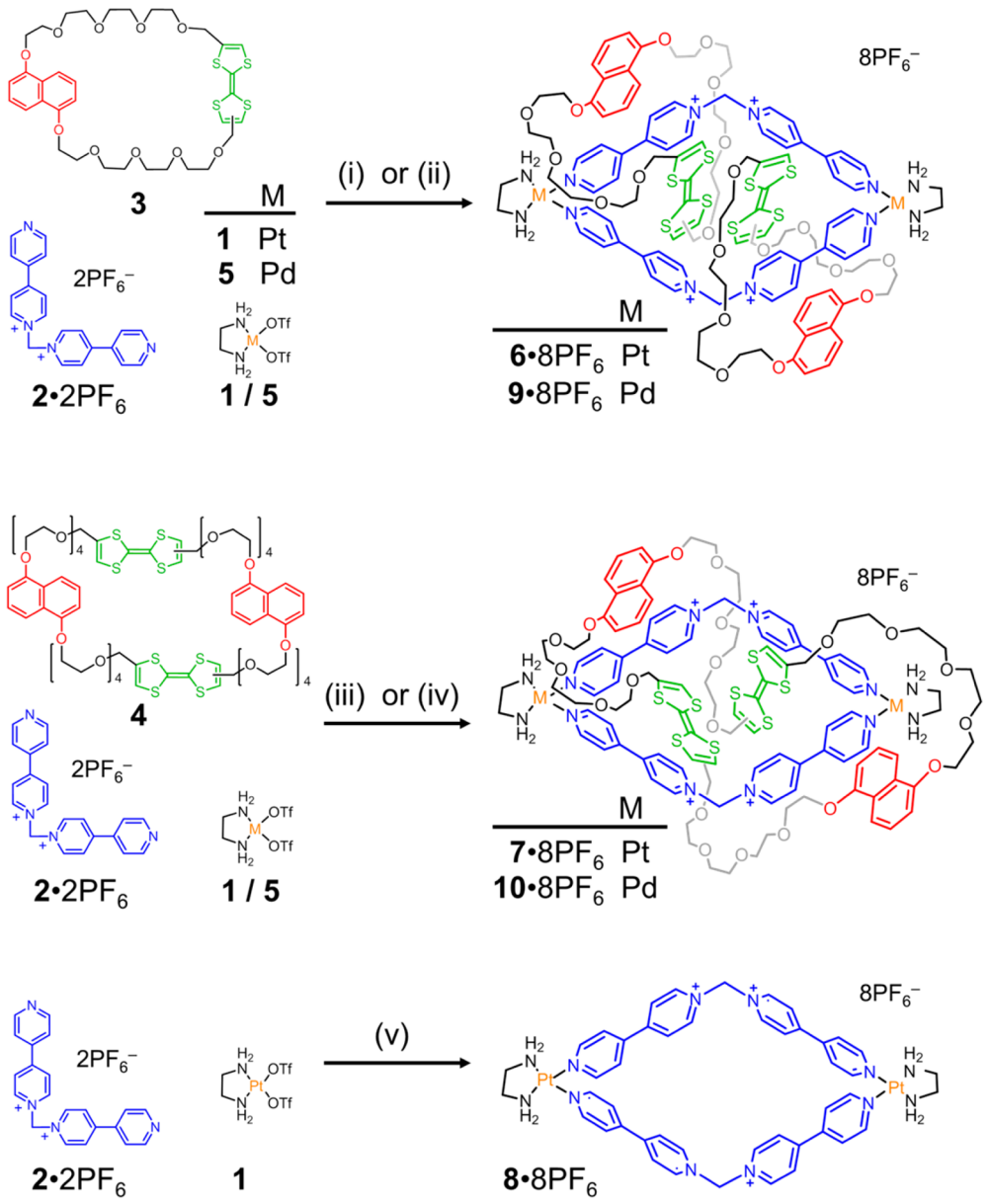

[a]**2**·2PF$_6$, **3**: (i) **1**, MeCN, 50 °C, 7 d, 34%; (ii) **5**, MeCN, rt, 1 h, quant. [b]**2**·2PF$_6$, **4**: (iii) **1**, MeCN, 50 °C, 7 d, 39%; (iv) **5**, MeCN, rt, 1 h, quant. [c]**2**·2PF$_6$: (v) **1**, MeCN, 50 °C, 7 d, 47%.

reveals unprecedented topological and mechanical control over TTF radical recognition processes. A more dramatic effect was observed within the topological isomers, that is, the Solomon link and the ring-in-ring complex, where the decomplexation of the {2+2} macrocycle **4** from the organoplatinum square **8**$^{8+}$ occurs spontaneously upon redox stimulation of the TTF units. All the experimental data, together with (4) supporting quantum mechanical calculations, *points to a fundamental connection between the topology of the molecules and their redox properties in addition to their geometries and constitutions.*

2. RESULTS AND DISCUSSION

2.1. Stereochemical Nomenclature. Central to the discussion in this article are three isomers.[35] They are (i) a [3]catenane, **6**$^{8+}$ (Figure 1b), (ii) a doubly interlocked [2]catenane or molecular Solomon link, **7**$^{8+}$ (Figure 1c), and (iii) a ring-in-ring complex **4⊂8**$^{8+}$ (Figure 1d). For the sake of convenience, we will refer to (i) **6**$^{8+}$ and (ii) **7**$^{8+}$ as mechanical/constitutional isomers,[36] (i) **6**$^{8+}$ and (iii) **4⊂8**$^{8+}$ as constitutional isomers,[37] and (ii) **7**$^{8+}$ and (iii) **4⊂8**$^{8+}$ as topological isomers.[38] All three isomers have their own discrete topologies, in addition to their well-defined geometries and constitutions.

2.2. Synthetic Protocols and Solid-State Characterizations. Template-directed strategies, driven by [$\pi\cdots\pi$] donor–acceptor and [C–H···O] interactions, constitute a common approach[14] to the preparation of mechanically interlocked molecules (MIMs). The formation of the [3]-catenane **6**·8PF$_6$ (Figure 1b) is templated by these interactions, and the interlocked structure is further held together[39] by platinum(II)–pyridine coordination bonds. Addition of the π-deficient ligand[40] **2**$^{2+}$ to the π-electron-rich {1+1} macrocycle **3**

dx.doi.org/10.1021/ja504662a | J. Am. Chem. Soc. 2014, 136, 11011–11026

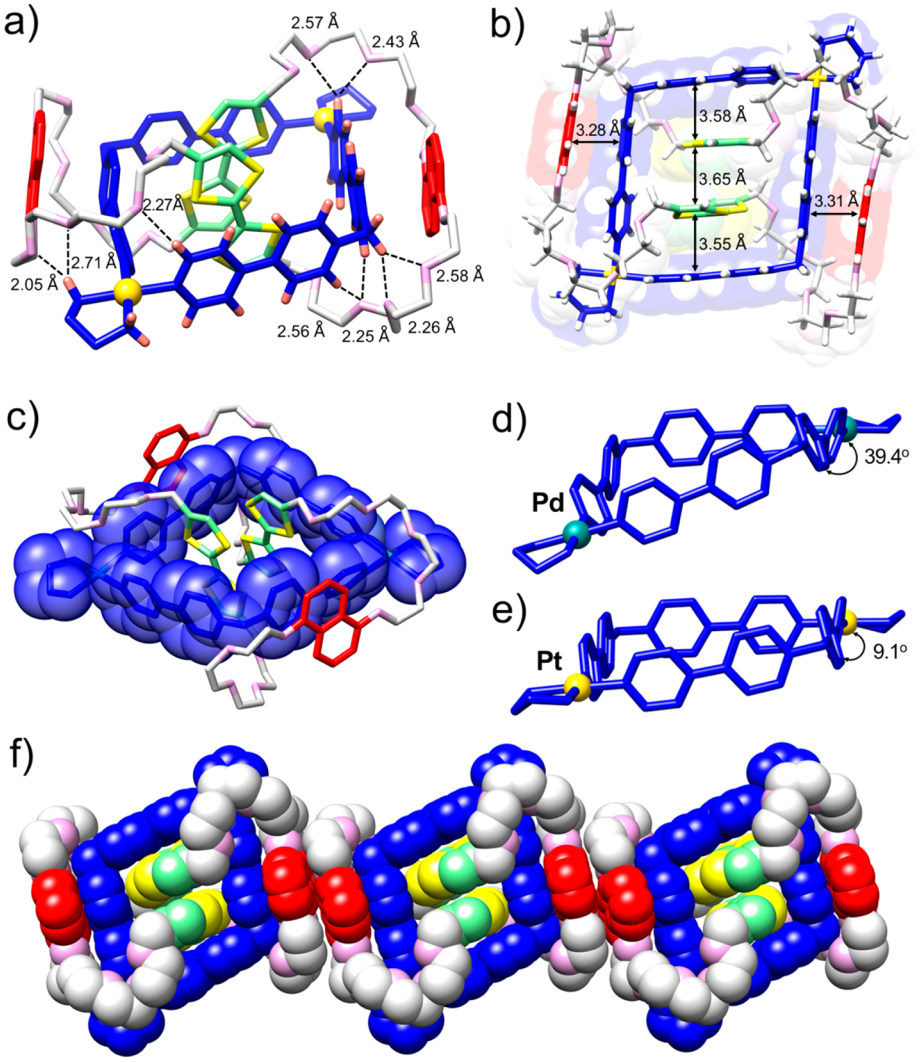

Figure 2. Side-on (a) and plan (b) views of the solid-state structure of the molecular Solomon link 7^{8+} showing (a) the [C−H···O] and [N−H···O] distances (Å) between the oxygen atoms of the polyether loop and the hydrogen atoms (orange) of the BIPY$^+$ unit, the methylene group, and the ethylenediamine moiety of the organoplatinum square and (b) the average [π···π] stacking distances between the BIPY$^+$ walls and the DNP and TTF units, as well as the interplanar spacing between the two tetrathiafulvalene units. Solvent molecules and PF_6^- counterions have been omitted for the sake of clarity. Only one enantiomer of the molecular Solomon link is shown. (c) Solid-state structure of the molecular Solomon link $\mathbf{10}^{8+}$ displaying the macrocyclic polyether mechanically interlocked within the distorted-square shaped organopalladium square. (d, e) Tubular representation of the organometallic square from the solid-state structures of the molecular Solomon links $\mathbf{7}^{8+}$ and $\mathbf{10}^{8+}$ showing the torsional angles of the 4,4′-C−C bond of the BIPY$^+$ unit. Side-on view of the organopalladium square, which exists in the crystal structures of $\mathbf{10}^{8+}$, showing the significant deviation from planarity compared with the organoplatinum square from the solid-state structure of $\mathbf{7}^{8+}$. (f) Space-filling representation of the long-range packing of the molecular Solomon link $\mathbf{7}^{8+}$.

in MeCN is accompanied by a change in the color of the reaction mixture to deep green, indicating the presence of a charge-transfer (CT) complex. The reaction of this complex with 2 equiv of the platinum complex **1** for 7 days at 50 °C resulted (Scheme 1), after counterion exchange, in the isolation of the [3]catenane $\mathbf{6}\cdot 8PF_6$ as a green solid in 39% yield. The syntheses of the molecular Solomon link $\mathbf{7}^{8+}$ was achieved (Scheme 1) in 34% yield by following a similar protocol, using the {2+2} macrocycle[41] **4**, which contains two TTF and two DNP units. See the Supporting Information for detailed synthetic procedures and characterization. For the sake of comparison, we have also employed palladium(II) square planar centers for the assembly of those mechanical/constitutional isomers. Indeed, by mixing the crown ether **3** or **4** with the pyridine-based ligand $\mathbf{2}\cdot 2PF_6$ and the ethylenediamine-chelated Pd(II) corner **5** (Scheme 1), we obtained quantitatively, under thermodynamic control at room temperature, the [3]catenane $\mathbf{9}\cdot 8PF_6$ and the molecular Solomon link $\mathbf{10}\cdot 8PF_6$.

The structures of the mechanical/constitutional isomers $\mathbf{6}^{8+}$ and $\mathbf{7}^{8+}$ were readily revealed by X-ray crystallographic analysis[42] performed on the deep green single crystals of each, obtained on the slow vapor diffusion of iPr$_2$O at 0 °C into MeCN solutions of the [3]catenane and the molecular Solomon link, respectively. The X-ray crystal structure (Figure 1c) of $\mathbf{7}^{8+}$ unveils[43] a molecular structure with C_2 symmetry wherein the two ring components are *doubly* interlocked in the topology of a Solomon link. Although this topology is intrinsically chiral, single crystals of this doubly interlocked [2]catenane were optically inactive as a consequence of the crystallization as a racemic mixture of equimolar amounts of *P* and *M* enantiomers (Figure S18 in the Supporting

dx.doi.org/10.1021/ja504662a | J. Am. Chem. Soc. 2014, 136, 11011−11026

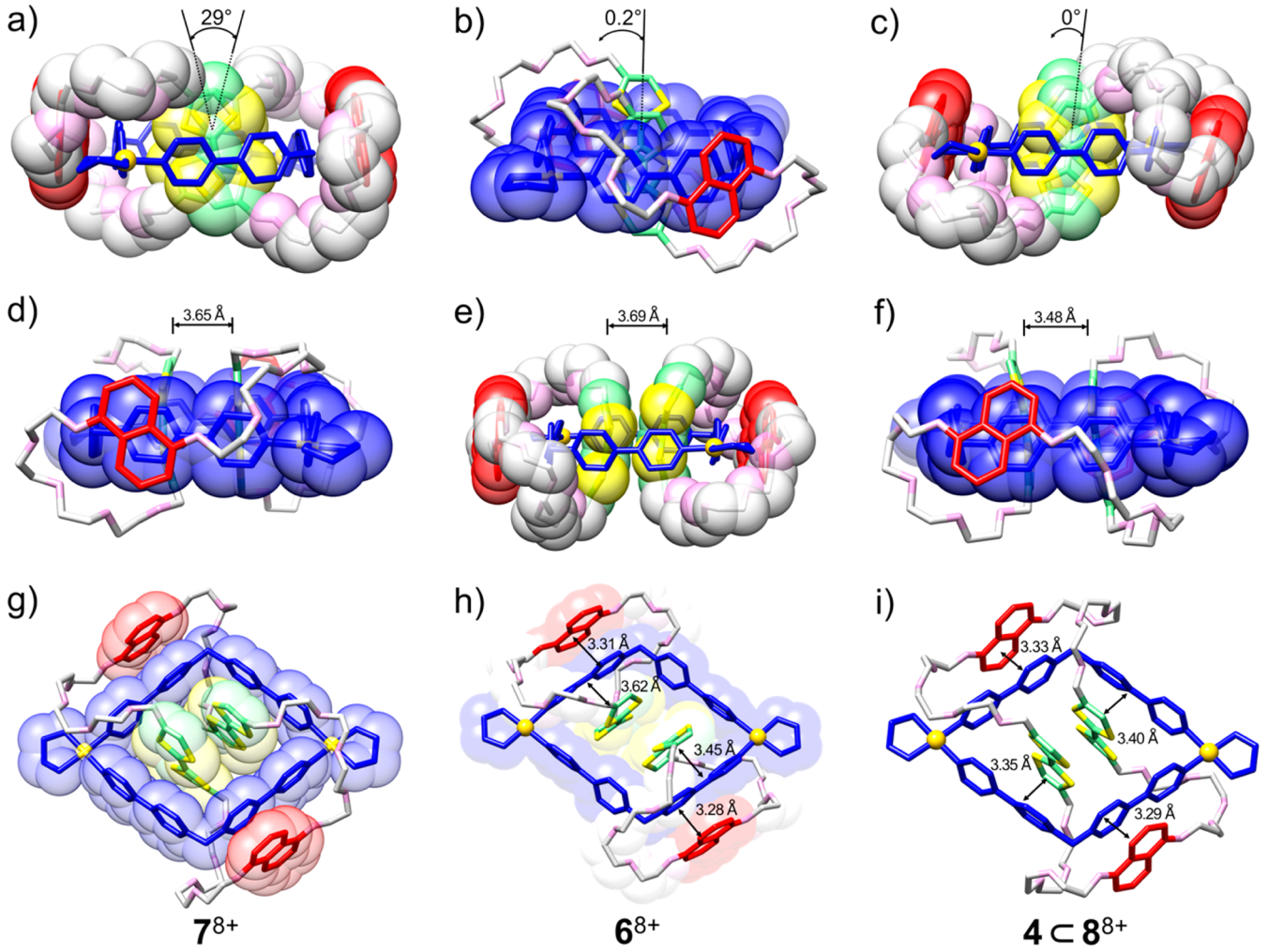

Figure 3. Solid-state structures of (a, d, g) the molecular Solomon link 7^{8+} and (b, e, h) the [3]catenane $\mathbf{6}^{8+}$, and the solid-state superstructure of (c, f, i) the ring-in-ring complex $\mathbf{4}\subset\mathbf{8}^{8+}$ obtained by single-crystal X-ray crystallography, displayed in two different side-on (top and middle) views and as a perspective (bottom) view. (a–c) The angles of offset of the TTF units, defined by the relative orientations of the C═C double bonds in the tetrathiafulvalene units, display the different geometrical arrangement of the TTF units within the molecular framework of the three isomers. The space-filling representation of the {2+2} macrocycle polyether, (a) doubly interlocked or (c) included in the organoplatinum square, in tubular format, highlights the different shape of the polyether chain within the molecular framework of the topological isomers, the molecular Solomon link 7^{8+}, and the ring-in-ring complex $\mathbf{4}\subset\mathbf{8}^{8+}$. (d–f) The average interplanar spacing between the two tetrathiafulvalene units included in the organoplatinum square. (g–i) The [$\pi\cdots\pi$] stacking interactions between the TTF and DNP units and the proximal $BIPY^+$ units of the organoplatinum square in the three isomers, displayed as tubular models along with average distances (h, i). The DNP and TTF units of the {1+1} macrocycle polyether of the [3]catenane $\mathbf{6}^{8+}$ participate in a parallel [$\pi\cdots\pi$] stacking disposition with the $BIPY^+$ walls of the molecular square. All hydrogen atoms, solvent molecules, and counterions have been removed for the sake of clarity.

Information). Both TTF units exist in their *trans* configurations, and the stabilization within the cavity of the organoplatinum square is aided and abetted by [$\pi\cdots\pi$] stacking and [C–H···O] interactions between some of the glycol oxygens and some of the bipyridinium ($BIPY^+$) hydrogen atoms. Close contacts (2.2–2.5 Å) exist (Figure 2a) between methylene protons and the oxygen atoms of the polyether chain in addition to [N–H···O] hydrogen bonds between the ethylenediamine hydrogens and the glycol oxygens (the average distance of N–O close contact pairs is 3.1 Å). The TTF units are involved (Figure 2b) in [$\pi\cdots\pi$] stacking interactions (interplanar separation, 3.65 Å) with the proximal $BIPY^+$ units. The less electron-rich DNP units take part in short proximal interplanar contacts (3.32 Å) with the outer faces of the $BIPY^+$ walls. The organoplatinum square of 7^{8+} is distorted with the four corners of the square being slightly noncoplanar. The out-of-plane distortion of the metallocycle is more evident (Figure 2c and Figure S21, Supporting Information) in the X-ray crystal structure of $\mathbf{10}^{8+}$, the palladium analogue of the molecular Solomon link.[44] The organopalladium square in the structure of $\mathbf{10}^{8+}$ has a rhombus-like shape, with the Pd atoms exhibiting the typical square planar coordination geometry, with an average distance for the Pd–N coordination of 2.05 Å. Moreover, the torsional angle in the proximal $BIPY^+$ unit in the organopalladium square (Figure 2d) is 39.4°, whereas that in the organoplatinum square (Figure 2e) is 9.1°. The distortion of the square in 7^{8+} is presumably in order to facilitate the [C–H···O] short contacts between the polyether chain and the $BIPY^+$ hydrogen atoms, an observation that is supported by the density functional theory (DFT) optimized structure (see Supporting Information) of a single 7^{8+} octacation, indicating that the forces associated with the crystal packing result in a more compact structure. Noncovalent bonding interactions help to sustain (Figure 2f) the extended superstructure of 7^{8+}.

dx.doi.org/10.1021/ja504662a | J. Am. Chem. Soc. 2014, 136, 11011–11026

A noteworthy interplay between the topology of the molecules and their geometries emerges (Figure 3) from the arrangement of the TTF units within the mechanically interlocked frameworks of 6^{8+} and 7^{8+}. The different noncovalent bonding interactions between the TTF units in the two structures are evidenced by a vertical offset of 29° for the TTF units in the case of molecular Solomon link 7^{8+} (Figure 3a), whereas the solid-state structure[45] of the [3]catenane 6^{8+} has the TTF units overlapping almost perfectly with a negligible (Figure 3b) angular offset of 0.2° and a vertical offset of 1.6 Å and an interplanar distance of 3.69 Å (Figure 3e). The interplanar separation between the encapsulated TTF units and the plane of the $BIPY^+$ walls of 6^{8+} range from 3.45 and 3.62 Å (Figure 3h). In addition, the DNP units participate in proximal interplanar contacts (3.28 Å) with the $BIPY^+$ moieties, which result (Figure 3h) in a parallel [$\pi\cdots\pi$] stacking disposition of six aromatic systems of the [3]catenane 6^{8+}. The values of the interplanar distance and the orientation of the tetrathiafulvalene units within the molecular framework of the [3]catenane 6^{8+} are very similar to those observed[46] in the solid-state structure of the [3]catenane 9^{8+} where the two TTF units are contained in the organopalladium square.

When 1 equiv of **4** was added to a MeCN solution of **8**·8PF_6, which was synthesized independently from its precursors, a deep green color, originating from a charge-transfer band centered on 856 nm, was observed. A binding constant of 1980 ± 75 L mol^{-1} between the two components of this ring-in-ring complex (Figure 1d) was determined by a UV−vis titration, which followed (Figure S42 in the Supporting Information) the characteristic green color change arising from the CT interactions between the two macrocycles. The binding mode of this complex was elucidated by X-ray diffraction of the single crystals isolated by slow vapor diffusion of Et_2O into a 1:1 mixture of **4** and **8**·8PF_6 in MeCN. The solid-state superstructure (Figure 3c) confirms[47] the existence of a ring-in-ring complex **4**⊂8^{8+}, the latter being a topological isomer of the molecular Solomon link 7^{8+}. The two electron-rich TTF units in the {2+2} macrocycle **4** are housed within the cavity of the organoplatinum square 8^{8+}, with an average distance of 3.48 Å between the mean planes of the TTF units (Figure 3f). The [$\pi\cdots\pi$] stacking interactions of the DNP units with the proximal electron-deficient $BIPY^+$ walls (mean interplanar distance of 3.31 Å, Figure 3i) are augmented by [C−H···O] close contacts and [N−H···O] hydrogen bonds involving the NH_2 groups of the ethylenediamine ligand and the glycol oxygens of the macrocyclic polyether. In common with the molecular Solomon link, the ring-in-ring complex displays a compact achiral superstructure.

2.3. NMR Spectroscopic Investigations. The solution-state characterizations of 6^{8+} and 7^{8+}, which were accomplished by using ^{1}H NMR and ^{13}C NMR spectroscopies, provide additional confirmation of their interlocked nature, as well as the relative positions of the organoplatinum square encircling the tetrathiafulvalene units in the ground state. The resonances, assigned by employing 2D NMR techniques (Figures S3, S6, and S7, Supporting Information), are consistent with the [3]catenane and the molecular Solomon link having the structure represented by 6^{8+} and 7^{8+}. Figure 4 presents a comparison of the chemical shift of the aromatic protons at 298 K of the molecular Solomon link 7^{8+} and [3]catenane 6^{8+} and their interlocked components, the {1+1} and {2+2} macrocyclic polyethers **3** and **4** and the bidentate dicationic ligand 2^{2+}. Most notable is the large upfield shift ($\Delta\delta_{TTF} \approx -0.33$ ppm) of the TTF proton resonances of 7^{8+}, which arises from the shielding effects of the aromatic walls of the square in keeping with the inclusion of the electron-rich TTF units within the organoplatinum square. The resonance corresponding to the α-protons of the $BIPY^+$ groups of the ligands coordinated to the metals is shifted significantly downfield ($\Delta\delta_{BIPY\text{-}\alpha} = +0.41$), as a consequence of metal−pyridine coordination. The shielding effect of the TTF and DNP units results in a significant upfield shift ($\Delta\delta_{BIPY\text{-}\beta} = 0.07-0.98$ ppm) of the resonances assigned to the β-protons on the $BIPY^+$ groups of the organoplatinum square. The resonances derived from the protons of the DNP units and the bridging methylene groups in the organoplatinum square show large separations as a result of the shielding and deshielding of the aromatic rings and their [C−H···O] interactions with the glycol chains. Additional [N−H···O] interactions with the glycol chains also result in the downfield shift of some resonances corresponding to the NH_2 protons on the ethylenediamine ligands. Since the

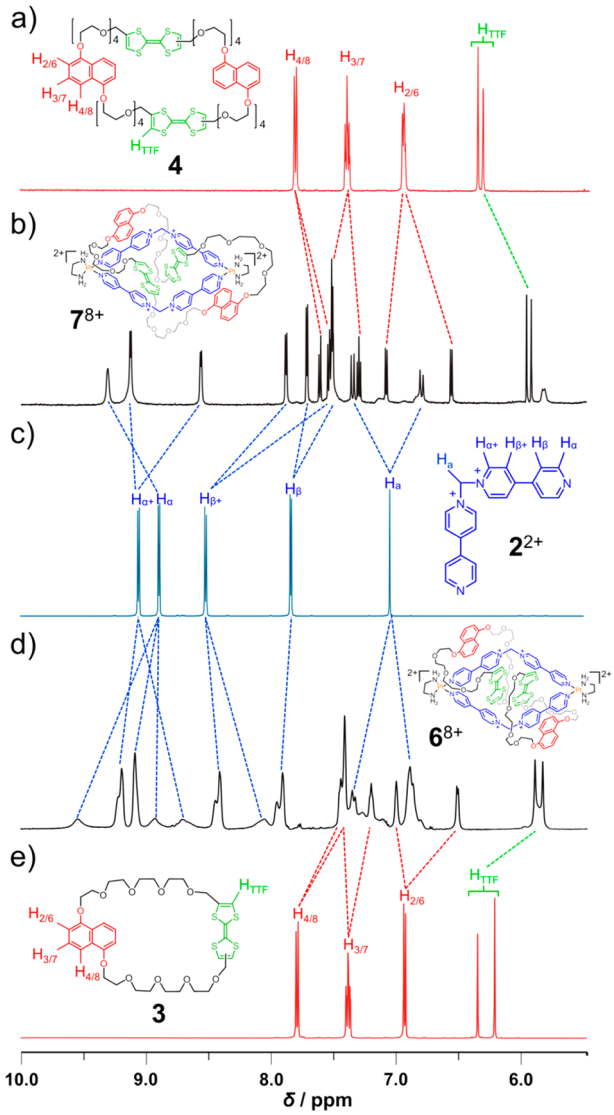

Figure 4. Partial ^{1}H NMR spectra (500 MHz, CD_3CN, 298 K) comparing the chemical shifts of the aromatic protons in (b) the molecular Solomon link 7^{8+} and (d) the [3]catenane 6^{8+} with those of (c) the bidentate dicationic ligand 2^{2+} and the macrocyclic polyethers (a) **4** and (e) **3**, which contain, respectively, four and two alternating TTF and DNP units.

dx.doi.org/10.1021/ja504662a | J. Am. Chem. Soc. 2014, 136, 11011−11026

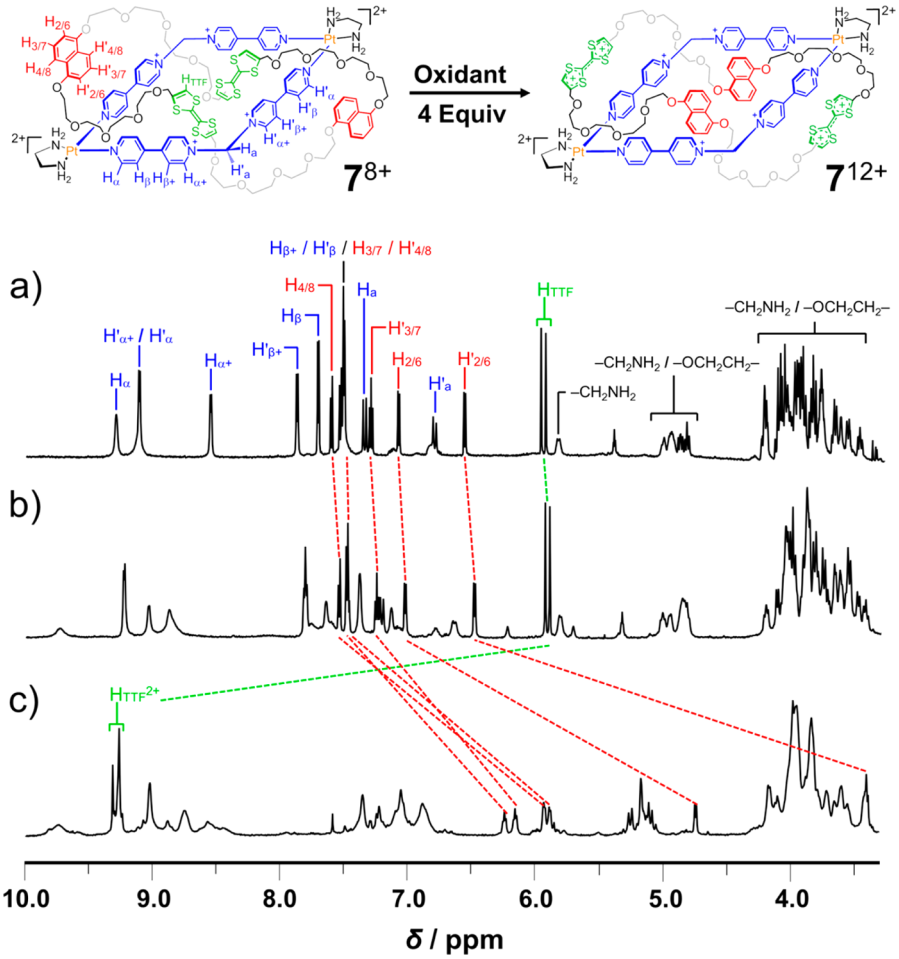

Figure 5. ^{1}H NMR spectra (600 MHz, CD_3CN) of the molecular Solomon link 7^{8+} recorded at (a) 298 K and (b) 233 K and (c) the fully oxidized 7^{12+} obtained after addition of 4 equiv of tris(4-bromophenylammoniumyl) hexachloroantimonate. The upfield shifts of the six DNP resonances are indicative of the location of the DNP units inside the organoplatinum molecular square upon complete oxidation and concomitant ejection of both TTF^{2+} dications to proximal locations. Assignments of the resonances have been confirmed with the assistance of data from 2D ^{1}H–^{1}H COSY experiments. See the Supporting Information.

rate of rotation of the $BIPY^+$ units of the organoplatinum square around their N–N axes is fast on the ^{1}H NMR time scale, only two sets of proton signals for the $BIPY^+$ units appear in the spectrum. Only one coconformation of the molecular Solomon link is observed at different temperatures in the ^{1}H NMR spectra (Figure 4b and Figure S2, Supporting Information) of 7^{8+}, namely, the one in which the TTF units are located inside the organoplatinum square. By contrast, the ^{1}H NMR spectrum (Figure 4d and Figures S9–S12, Supporting Information) of 6^{8+} is commensurate with the expected[33,40a] distribution of coconformations, which equilibrate slowly on the ^{1}H NMR time scale. Upon performance of variable temperature experiments, the resonances separate into a set of distinct signals at 233 K, pointing to the existence of dynamic processes within this [3]catenane.

The redox-stimulated switching of the molecular Solomon link was probed by ^{1}H NMR spectroscopy, using tris(4-bromophenylammoniumyl)hexachloroantimonate as the chemical oxidant. Complete oxidation of the TTF units, following the addition of 4 equiv of the oxidant to form 7^{12+}, results in substantial changes (Figure 5) in the ^{1}H NMR spectrum. Analysis by diffusion-ordered ^{1}H NMR spectroscopy reveals (Figure S29 in the Supporting Information) the presence of a single band corresponding to a diffusion coefficient of 1.6×10^{-10} $m^2 \cdot s^{-1}$, a value that is close to that measured for the 7^{8+} state, confirming that only one species is present in solution following oxidation. The oxidation of both TTF units to their dicationic forms was confirmed by the downfield shift of about 4 ppm for the resonances of the aromatic tetrathiafulvalene protons. The two peaks, corresponding to the formation of TTF^{2+} units, can be identified between 9.2 and 9.4 ppm. This change in the ^{1}H NMR spectrum is accompanied by an upfield shift of the resonances associated with the DNP protons. In particular, the H-2/6 protons of the DNP units resonate further upfield at 3.3 and 4.7 ppm as a consequence of shielding effects from the $BIPY^+$ units in the organoplatinum square. Other peaks, corresponding to the remaining DNP protons, also resonate further upfield. Examination of the ^{1}H-COSY spectrum (Figures S26–S28, Supporting Information) for the oxidized molecular Solomon link shows the coupling between the aromatic protons of the DNP units clearly. The chemical shift changes of the resonances for TTF and the DNP units indicate that the DNP units move inside the cavity of the organoplatinum square upon four-electron oxidation, in concert with the TTF^{2+} units being ejected as a consequence of Coulombic repulsion.

2.4. Electrochemical Studies. The redox behavior of the TTF moieties within the organoplatinum square of the three

dx.doi.org/10.1021/ja504662a | J. Am. Chem. Soc. 2014, 136, 11011–11026

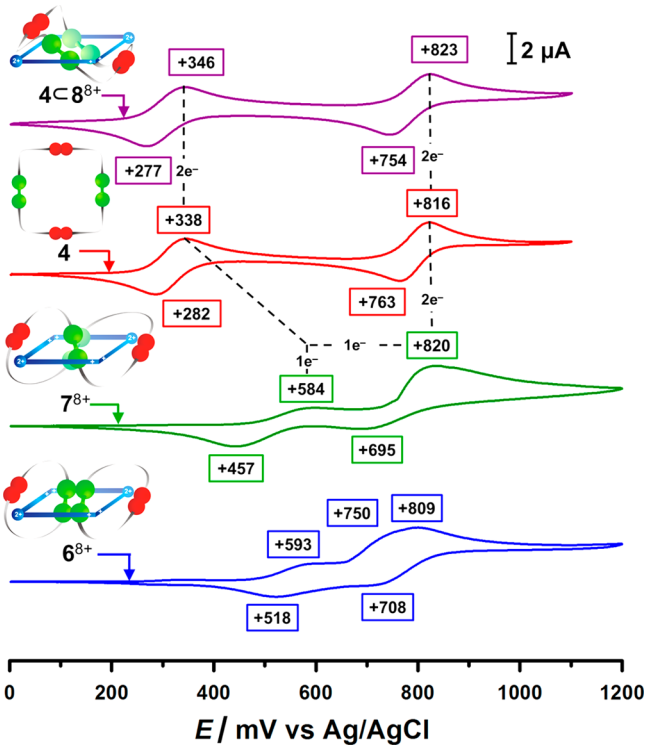

Figure 6. Cyclic voltammograms (1 mM in MeCN, 100 mM $TBAPF_6$, 10 $mV{\cdot}s^{-1}$, 298 K) of the ring-in-ring complex $\mathbf{4}\subset\mathbf{8}^{8+}$ (purple curve), the TTF-containing macrocyclic polyether **4** (red curve), $\mathbf{7}{\cdot}8PF_6$ (green curve), and $\mathbf{6}{\cdot}8PF_6$ (blue curve). From the integration of the oxidation peaks for $\mathbf{7}^{8+}$, the first process is a one-electron and the second process a three-electron one. Compared with the topological isomer, the ring-in-ring complex $\mathbf{4}\subset\mathbf{8}^{8+}$, the first oxidation peak for $\mathbf{7}^{8+}$ is shifted to a higher oxidation potential, indicating the formation of a stable mixed-valence $(TTF_2)^{\bullet+}$ state. The second oxidation process for $\mathbf{6}^{8+}$ is shifted by 70 mV toward more negative potentials, compared with the second oxidation peak of $\mathbf{7}^{8+}$, an indication that the formation of a radical-cationic $(TTF^{\bullet+})_2$ dimer occurs inside the organoplatinum square in the [3]catenane.

isomers under investigation was also probed electrochemically.[48] Cyclic voltammetry (CV) shed further understanding (Figure 6) on the redox-controlled *reptation* of the macrocyclic polyether within the molecular Solomon link. The oxidative region of the voltammogram of $\mathbf{7}^{8+}$ displays a one-electron process at +584 mV versus Ag/AgCl and a broad anodic peak centered on +820 mV that can be assigned to a three-electron process, as evaluated (Figure S34, Supporting Information) from chronocoulometry. The removal of the four electrons associated with the two TTF units of the free macrocyclic polyether **4** occurs as two two-electron processes with anodic peak potentials at +338 and +816 mV. The reduction scan of $\mathbf{7}^{12+}$, starting with the two tetrathiafulvalene units in their dicationic state, occurs as two two-electron processes centered at +695 and +475 mV. When the CV is switched at a vertex potential between the first and the second peak (Figure S30 and S31, Supporting Information), the resulting reduction peak is only a one-electron process. The first oxidation event of $\mathbf{7}^{8+}$ indicates that a stabilized species is formed upon the ejection of one electron from the TTF^0 unit, suggesting the generation of the mixed-valence $(TTF_2)^{\bullet+}$ dimer as a result of the close proximity of the two TTF groups in the spatially restricted cavity of the organoplatinum square. This process is followed by a one-electron oxidation to form two radical-cationic $TTF^{\bullet+}$ units, a transition that is shifted to substantially more positive potentials and is similar to the potentials observed[32c,33] for the second oxidation of "free" TTF species. Indeed, this anodic process shows only one broad peak around +820 mV, which includes the one-electron oxidation from the mixed-valence $(TTF_2)^{\bullet+}$ state to the bis-radical dication $(TTF)_2^{\bullet+}$ state, and the subsequent two-electron oxidation of the $TTF^{\bullet+}$ units to TTF^{2+} dications. Unlike the mixed-valence state $\mathbf{7}^{9+}$, any potential stabilization provided by radical dimerization in $\mathbf{7}^{10+}$ does not overcome the forces of electrostatic repulsion, resulting in the rapid ejection of both $TTF^{\bullet+}$ units from the cavity of the octacationic organoplatinum square. This translocation process leaves the second oxidation of the tetrathiafulvalene units to occur at the same potential as would be the case in the absence of the organoplatinum square.

The destabilizing interactions associated with the inclusion of the positively charged $TTF^{\bullet+}$ radical cations within the octacationic square cause the concerted translation of the $TTF^{\bullet+}$ and DNP units around the molecular Solomon link in order to reach a stable geometry where the DNP units are located within the cavity. Because the organoplatinum square has some affinity for the DNP units, reduction of the TTF units to their neutral states does not immediately return the molecule to its ground state coconformation.[30a,49] As consequence of the topological constraints imposed on the molecule, the Solomon link relaxes slowly from a metastable state coconformation to encircle the neutral electron-rich TTF units in preference to the DNP ones, by slow *reptation* of the macrocyclic polyether around the organoplatinum square.

Electrochemical investigation performed on the topological isomer, namely, the inclusion complex of the macrocyclic polyether **4** and the organoplatinum square $\mathbf{8}^{8+}$, indicates that, upon oxidation of the TTF units, the binding of the macrocyclic polyether within the square is completely eradicated. In this case, the two oxidation events correspond exactly with those observed for the macrocyclic polyether alone, suggesting that the mixed-valence $(TTF_2)^{\bullet+}$ state is not stabilized as a result of complexation within the organoplatinum square. Hence, it is the interlocked nature of the molecular Solomon link architecture that leads to the stability of the mixed-valence state compared with the topologically isomeric ring-in-ring complex, thus highlighting the profound consequences of topology on molecular properties. The redox properties of the molecular Solomon link $\mathbf{7}^{8+}$ were then compared with the mechanical/constitutional isomer, that is, the [3]catenane $\mathbf{6}^{8+}$. The complete potential scan for $\mathbf{6}^{8+}$ reveals a one-electron oxidation at +593 mV, which is assigned to the mixed-valence state. Unlike the molecular Solomon link, the one-electron oxidation to form two radical-cationic $TTF^{\bullet+}$ units in the [3]catenane, which occurs at a peak potential of +750 mV, can be easily distinguished (Figure 6 and Figure S32, Supporting Information) from the subsequent oxidation to the TTF^{2+} dications at +809 mV, and it is shifted 70 mV toward more negative potentials compared with the oxidation peak for $\mathbf{7}^{8+}$. This observation indicates that in the [3]catenane, in stark contrast to the molecular Solomon link, the two $TTF^{\bullet+}$ radical cations are stabilized through the formation of a radical-cation dimer inside the organoplatinum square, despite the electrostatic repulsion that they must experience in that position.

The existence of a transient regime in the molecular Solomon link between the $\mathbf{7}_{in}^{10+}$ state, where both $TTF^{\bullet+}$ units are housed within the cavity of the organoplatinum square and the $\mathbf{7}_{out}^{10+}$ state, in which both of them leave the cavity on

dx.doi.org/10.1021/ja504662a | J. Am. Chem. Soc. 2014, 136, 11011−11026

account of destabilizing electrostatic interactions, was investigated by variable scan-rate CV. See Figure S31 in the Supporting Information. The first oxidation peak of 7^{8+} is totally reversible and independent of the scan rate, as the result of the formation of a stable state, the mixed-valence $(TTF_2)^{\bullet+}$ dimer, upon one-electron oxidation of the molecular Solomon link. The second redox peak displays, however, scan-rate dependent behavior, a condition that suggests the presence of a transient state. At relatively low scan-rates, a broad oxidation peak is observed at +809 mV, which is found to be a three-electron process. If insufficient time is given for the ejection of two radical-cation $TTF^{\bullet+}$ units from the molecular square to occur, achieved by scanning the potential at progressively higher scan rates, oxidation to the TTF^{2+} state takes place *inside* the octacationic square. This phenomenon results in the decrease of the intensity of the second oxidation peak, which is also accompanied by a shift toward more positive potentials, which indicates the existence of the 7_{in}^{10+} state. We hypothesize that this transient state, despite the destabilizing Coulombic repulsions associated with the inclusion of positively charged $TTF^{\bullet+}$ units within the octacationic molecular square, results from the highly constrained environment of the molecular Solomon link topology. Indeed, the topological constraint introduces a kinetic barrier to the *reptation* of the crown ether around the square to reach a more stable state, namely, the one in which both DNP units are located inside the structural framework of the organoplatinum square. The fact that the topology of the molecule has consequences for the kinetics of the switching process becomes even more evident from the comparison of the variable scan-rate voltammograms of the molecular Solomon link with the [3]catenane. Upon scanning a solution of $\mathbf{6}^{8+}$ at progressively faster scan rates, the second oxidation peak, namely, the one where the oxidation of radical cation $TTF^{\bullet+}$ units to TTF^{2+} dications occurs, exhibits a shift only in the fast scan regime (>1 V s^{-1}). Indeed, once the potential is scanned faster, a higher population of the radical dicationic $(TTF^{\bullet+})_2$ dimer can be detected within the cavity of the molecular square. In comparison with the 7^{10+} state of the molecular Solomon link, where the expulsion of the radical cation $TTF^{\bullet+}$ from the cavity of the molecular square is faced with a high energy barrier on account of the slow *reptation* of the macrocycle, the radical dicationic $(TTF^{\bullet+})_2$ dimer in the $\mathbf{6}^{10+}$ state encounters a lower kinetic barrier. Kinetic control over the geometrical changes emerges upon electronic stimulation of the tetrathiafulvalene units in these two mechanically interlocked molecules, a phenomenon that is consistent with the constraints imposed by the mechanical bonds within the two mechanical/constitutional isomers.

In order to account for the oxidation events in the molecular Solomon link, a mechanism is proposed (Figure 1c) wherein the TTF units in 7^{8+} are oxidized individually in three steps. The electronic spectra, associated with the electrochemical oxidation processes of 7^{8+} in MeCN (with 100 mM $TBAPF_6$), have been recorded (Figure 7a and Figure S36, Supporting Information) in order to shed more light on the intervalence transitions occurring within this structure. When the voltage of the working electrode is set at +700 mV (vs Ag/AgCl), the distinctive[33] absorbance of the TTF–$BIPY^+$ CT band centered at 860 nm in 7^{8+} decreases, while absorption bands at 620 and 437 nm, which are characteristic of the $TTF^{\bullet+}$ state, appear in the spectrum. Also, a new broad absorption band in the NIR emerges at ca. 2000 nm. This broad band can be attributed[32,33] to the formation of a mixed-valence state between two

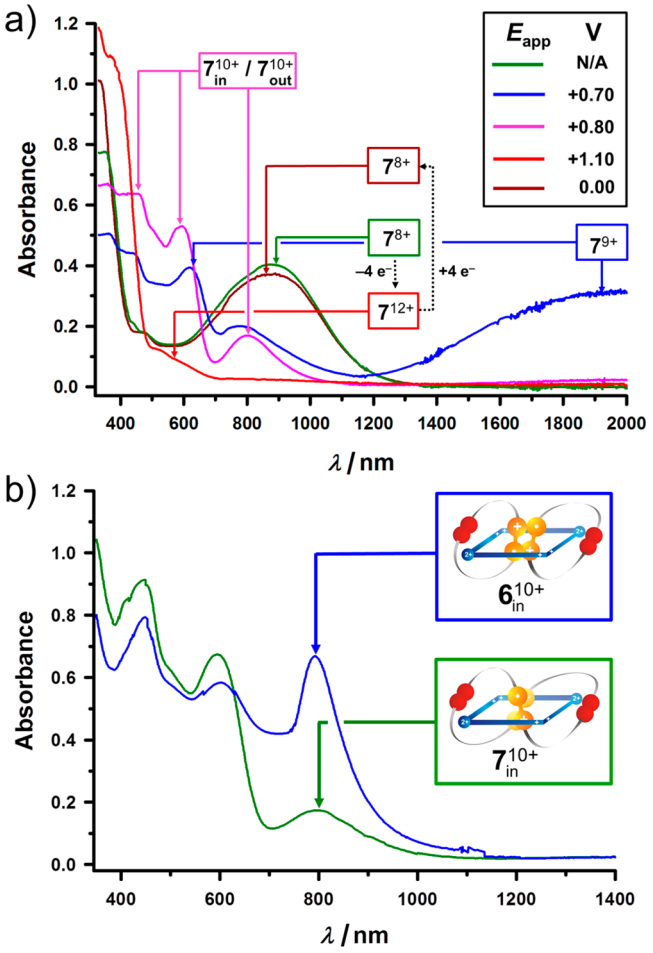

Figure 7. (a) UV–vis–NIR spectroelectrochemistry of $\mathbf{7}\cdot 8PF_6$ (0.15 mM in MeCN, 100 mM $TBAPF_6$, 298 K) and the oxidized states arising from the electrochemical oxidation at different applied potentials (E_{app}). (b) Comparison of the UV–vis–NIR absorption spectra of solutions (0.15 mM in MeCN) of $\mathbf{6}\cdot 8PF_6$ (blue curve) and $\mathbf{7}\cdot 8PF_6$ (green curve) recorded upon the addition of up to 2.0 equiv of $Fe(ClO_4)_3$ as the chemical oxidant.

tetrathiafulvalene units. The stability of the mixed-valence $(TTF_2)^{\bullet+}$ state in 7^{9+} is not affected by electrostatic destabilization within the octacationic molecular square, an observation that is corroborated by the emergence of the characteristic radical signal in the electron paramagnetic resonance (EPR) spectrum (Figure S40 in the Supporting Information). The conversion to 7^{10+}, which was achieved by applying a potential of +800 mV, results in the complete disappearance of the NIR absorption band and an increase in the bands of the $TTF^{\bullet+}$ state. A very small absorption band was observed at 800 nm, a region that is usually related[33] to the generation of the radical-cationic dimer $(TTF^{\bullet+})_2$ state. In contrast to 7^{10+}, an oxidative TTF dimerization process occurs (Figure 7b) for the $\mathbf{6}^{10+}$ of the [3]catenane, as indicated by the presence of a much stronger absorption $(TTF^{\bullet+})_2$ radical-cation dimer band, a phenomenon that can be ascribed as consequence of the higher flexibility of the TTF radical cations in the {1+1} macrocycles in $\mathbf{6}^{8+}$, which allows an efficient orbital overlap between the tetrathiafulvalene units. Shifting the potential to +1100 mV so as to obtain 7^{12+} led to the appearance of the characteristic TTF^{2+} absorption band at 370 nm, along with the emergence of a new absorption band at 600

dx.doi.org/10.1021/ja504662a | J. Am. Chem. Soc. 2014, 136, 11011–11026

nm as a result of the CT interaction between the walls of the organoplatinum square and the newly encircled DNP units. The fact that the electrochemical switching of the molecular Solomon link is reversible is demonstrated by the restoration of the original spectrum of 7^{8+} after reduction by holding the potential at 0 V for 1 h.

2.5. EPR Experiments. Continuous wave (CW) EPR spectroscopy was used to investigate the behavior of the molecular Solomon link and the [3]catenane as a function of the oxidation states generated by electrochemical oxidation or by titrating the chemical oxidant $Fe(ClO_4)_3$ into a MeCN solution of $7{\cdot}8PF_6$ and $\mathbf{6}{\cdot}8PF_6$. Upon stepwise addition of the oxidant, significant differences in the EPR spectra of the [3]catenane and the molecular Solomon link were revealed (Figure 8). A gradual increase in the radical signal intensity of both 7^{8+} and $\mathbf{6}^{8+}$ was observed upon addition of the $Fe(ClO_4)_3$.

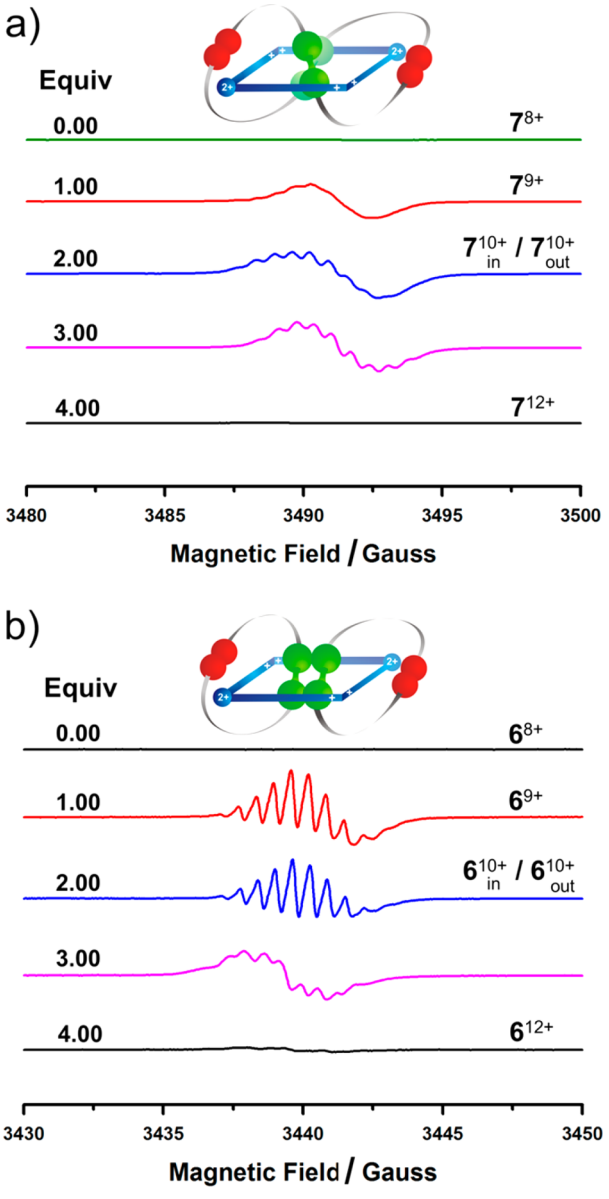

Figure 8. Continuous-wave EPR spectra of (a) molecular Solomon link 7^{8+} and (b) [3]catenane $\mathbf{6}^{8+}$ (0.20 mM in MeCN, 298 K) recorded upon the addition of 1.00, 2.00, 3.00, and 4.00 equiv of $Fe(ClO_4)_3$.

Titration with up to 1.0 equiv of $Fe(ClO_4)_3$ yielded (Figure 8a) an asymmetric derivative curve for 7^{8+} in which the lower field showed hyperfine interactions, while the higher field showed none. In contrast, the addition of 1.0 equiv of $Fe(ClO_4)_3$ to a solution of $\mathbf{6}{\cdot}8PF_6$ results (Figure 8b) in an EPR spectrum with a strong hyperfine splitting pattern superimposed on the spectral envelope. The hyperfine splitting observed for the mixed-valence $(TTF_2)^{\bullet+}$ dimer in $\mathbf{6}^{9+}$ is more symmetric and resolved compared with the ones observed in the spectra of the molecular Solomon link in the 7^{9+} state. A similar asymmetric behavior in the EPR spectrum has been observed previously for a mixed-valence $(TTF_2)^{\bullet+}$ dimer generated within a self-assembled coordination cage[37] and is believed to be a consequence of slow molecular motions on account of the locked geometry of the molecule.[50] Thus, the hyperfine splitting pattern of the EPR signal provides a qualitative indication of the extent to which the mixed-valence $(TTF_2)^{\bullet+}$ dimer moiety is contained in the organoplatinum square of the molecular Solomon link. In order to shed more light on the oxidation events of 7^{8+}, we performed (Figure 9a) a stepwise titration with $Fe(ClO_4)_3$ around the generation of the mixed-valence $(TTF_2)^{\bullet+}$ dimer in the molecular Solomon link. Below 1.0 equiv of oxidant added, which accesses the oxidation profile from TTF^0 to $(TTF_2)^{\bullet+}$, both TTF units are restricted within the organoplatinum square of the molecular Solomon link, yielding an asymmetric EPR spectrum. Above 1.0 equiv of oxidant added, in the redox window from 7^{9+} to 7^{10+}, the $TTF^{\bullet+}$ units are expelled from the organoplatinum square and become significantly less restricted in their motion, resulting in a more traditional, symmetric EPR spectrum after complete oxidation of the two tetrathiafulvalene units to their radical-cationic dimer $(TTF^{\bullet+})_2$ state, with the concomitant increase in the signal intensity. In order to confirm that the asymmetry in the EPR signal in the mixed-valence state of the molecular Solomon link does not arise because of interactions with the chemical oxidant, CW EPR spectroscopy was performed (Figure 9b) on the singly oxidized species, generated electrochemically by holding the potential for 30 min at +0.70 V versus Ag/AgCl. In the case of the [3]catenane $\mathbf{6}^{9+}$, the large range of coconformational freedom experienced by the tetrathiafulvalene units, as a consequence of the lower topological constraints in this constitution, results in a higher tumbling motion of the $TTF^{\bullet+}$ species and therefore in a more well-defined and symmetric hyperfine structure of the EPR signal (Figure 8b) in the mixed-valence $(TTF_2)^{\bullet+}$ for the $\mathbf{6}^{9+}$ state. A slight attenuation of the signal occurred upon oxidation of both TTF^0 units to their radical-cationic state, which is the result of the stronger spin-coupling upon generation of the radical-cationic dimer $(TTF^{\bullet+})_2$ state in $\mathbf{6}_{in}^{10+}$. In agreement with the electrochemical experiments, the radical-cation dimer $(TTF)_2^{\bullet+}$ state in $\mathbf{6}_{in}^{10+}$ state is in equilibrium with the $\mathbf{6}_{out}^{10+}$ state. Addition up to 4 equiv of $Fe(ClO_4)_3$ results in the formation of completely oxidized species, containing TTF^{2+} dications, which have no radical character and are EPR silent. The changes in the EPR spectra provide further evidence for the proposed topological effects on the dynamics of the molecule in solution upon successive oxidation of the tetrathiafulvalene units and hence on its radical recognition properties.

2.6. Solid-State Characterization of Mixed-Valence States. In order to probe in more detail the structural changes of these tetrathiafulvalene dimers within the organoplatinum square in the different topologies, we have grown single crystals

dx.doi.org/10.1021/ja504662a | J. Am. Chem. Soc. 2014, 136, 11011−11026

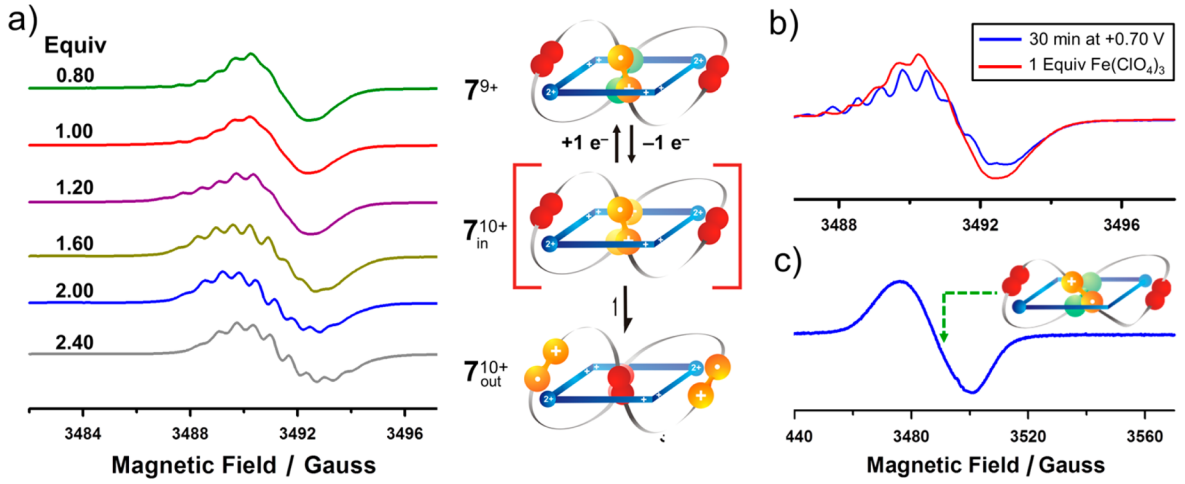

Figure 9. (a) CW EPR spectra of $7{\cdot}8PF_6$ (0.20 mM in MeCN, 298 K), recorded during a stepwise titration with $Fe(ClO_4)_3$ from 0.80 to 2.40 equiv. The spectra have been normalized for the sake of clarity. (b) CW EPR spectra of $7{\cdot}8PF_6$ (0.20 mM in MeCN, 298 K) recorded after electrolysis (blue curve) for 30 min at +0.70 V versus Ag/AgCl under an argon atmosphere and upon the addition (red curve) of 1.0 equiv of $Fe(ClO_4)_3$. (c) Solid-state CW EPR spectrum of a single crystal of $7{\cdot}7PF_6{\cdot}2ClO_4$, demonstrating the monoradical mixed-valence state of the tetrathiafulvalene units in the solid-state structure in accordance with the presence of nine counterions observed by the X-ray crystallography.

of the molecular Solomon link in the mixed-valence $(TTF_2)^{\bullet+}$ state 7^{9+} and also of 6^{9+}, the mixed valence $(TTF_2)^{\bullet+}$ dimer derived from the [3]catenane. Addition of 1.0 equiv of $Fe(ClO_4)_3$ into a MeCN solution of $6{\cdot}8PF_6$ or $7{\cdot}8PF_6$, followed by the slow vapor diffusion of Et_2O at 0 °C produced single crystals suitable for X-ray diffraction analysis.[51,52] In the case of the molecular Solomon link, the presence of nine counterions,[53] seven PF_6^- and two ClO_4^-, points to an oxidation state in which one of the two tetrathiafulvalene units is in the radical-cationic state. The existence of a monoradical state in the crystals of 7^{9+} is reinforced also by solid-state CW-EPR spectroscopy. The isotropic EPR spectrum (Figure 9c) of some single crystals suggests that the TTF dimers in the molecular Solomon link are paramagnetic in nature, an observation that confirms that the mixed-valence state of 7^{9+} is maintained in the solid state.

The interplanar distances between the TTF units and the angles of their offset obviously differ when comparing the solid-state structures of 7^{8+} with 7^{9+}. The interplanar distance (3.65 Å) between the neutral TTF^0 units in 7^{8+} changes dramatically upon oxidation to the mixed-valence $(TTF_2)^{\bullet+}$ state 7^{9+}, wherein the TTF units are separated (Figure 10a) by only 3.51 Å, in agreement with previously reported[33] solid-state structures of mixed-valence TTF dimers. This observation, along with the fact that the planarity of the TTF units increases while the angle of TTF offset decreases from 29° to 19°, reveals the existence of interactions between the TTF units in the 7^{9+} state arising from the delocalized nature of the single radical in the dimer. Of even greater interest, however, are the relative geometries adopted by TTF units in their mixed-valence states in compounds with different topologies. The crystal structure (Figure 10b and Figures S23 and S24, Supporting Information) of the radical cation mixed-valence 6^{9+} has its TTF units overlapping almost perfectly with no angular and vertical offset, a situation which allows an efficient orbital overlap and electron delocalization between the tetrathiafulvalene units in the radical state. The significance of the unique environment the TTF moieties experienced in the context of mechanical/constitutional isomers, that is, the [3]catenane and the molecular Solomon link, is highlighted here when analyzing the solid-state

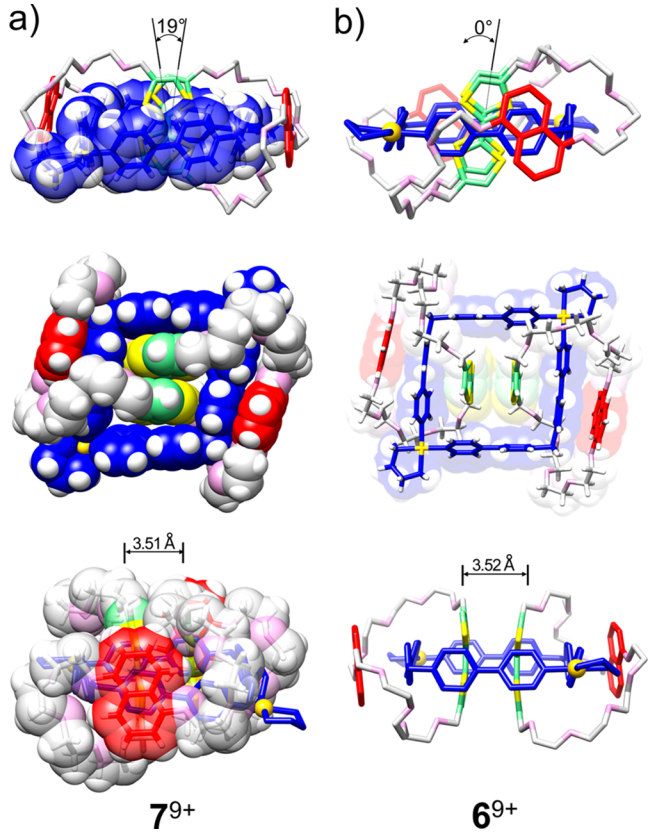

Figure 10. Solid-state structures of the tetrathiafulvalene mixed-valence states of (a) the molecular Solomon link 7^{9+} and (b) the [3]catenane 6^{9+} displayed as two different side-on (top and bottom) views and a plan (middle) view. Only one enantiomer of the Solomon link, which has topological chirality, is shown. In each case, the average interplanar spacings between the two tetrathiafulvalene units and the angles of offset are also shown to highlight the different geometrical relationships between the two TTF units positioned side-by-side inside the organoplatinum square for the stable mixed-valence $(TTF)_2^{\bullet+}$ states in 7^{9+} and 6^{9+}. The solvent molecules and counterions have been omitted for the sake of clarity.

dx.doi.org/10.1021/ja504662a | J. Am. Chem. Soc. 2014, 136, 11011−11026

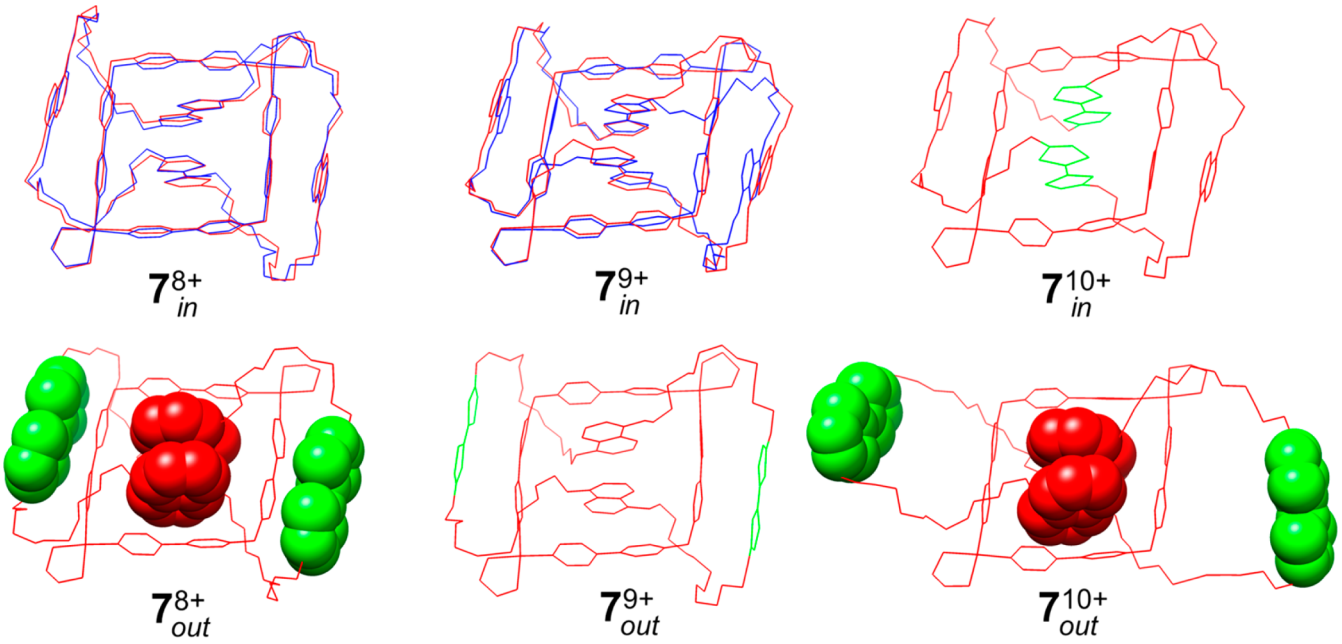

Figure 11. Graphical representation of the DFT-calculated structures and X-ray crystal structures of the molecular Solomon link. Calculated structures for the oxidized states 7^{8+} (left), 7^{9+} (middle), and 7^{10+} (right) with the two tetrathiafulvalene units housed within the cavity of the organoplatinum square (*in* coconformation) and the state in which both of them leave the cavity (*out* coconformation). The *in* coconformations for the 7^{8+} and 7^{9+} determined from theoretical calculation (red skeleton) are overlaid with the X-ray crystal structures of the molecular Solomon link (blue skeleton) in the corresponding redox state.

structures of TTF units and arises from the interface of mechanical effects upon radical recognition processes.

2.7. Computational Studies. Finally, quantum-mechanical modeling was used to investigate the stability of the species found in the different oxidation states of the [3]catenane and the molecular Solomon link. Density functional theory (DFT) at the level of M06/6-311G**++//M06-L/6-31G* with Poisson–Boltzmann solvation model[54] results in the predicted geometries[55] for the oxidation states $\mathbf{6}^{8+}$ and $\mathbf{6}^{9+}$ of the [3]catenane and the 7^{8+} and 7^{9+} of the molecular Solomon link (Figure 11) with the tetrathiafulvalene units adopting relative geometries that are almost identical to those observed in the X-ray crystal structures. Indeed, the comparison of the calculated structures with the experimental solid-state structures for those oxidation states reveals very similar values for the interplanar distances and the orientation of the tetrathiafulvalene units. A hypothetical coconformation, 7_{out}^{8+}, with two DNP units inside the organoplatinum square was also evaluated and its theoretical relative energy suggests that the coconformation with the TTF units inside the organoplatinum square is favored by 2.4 kcal mol^{-1}, supporting the experimental observations. For the [3]catenane, the coconformation $\mathbf{6}_{out}^{8+}$ with the DNP inside the organoplatinum square is less stable than the TTF-in coconformation by 1.5 kcal mol^{-1} (Table S1 in the Supporting Information). The calculation for the 7^{9+} state results in a more stable TTF-in coconformation than the DNP-in by 5.4 kcal mol^{-1}, even although the former is characterized by unfavorable electrostatic interactions. This result indicates that the interaction between $(TTF_2)^{\bullet+}$ dimer within the molecular Solomon link is strong enough to overcome the repulsion between the positive charge on the mixed-valence dimer and the octacationic organoplatinum square. A similar interaction between $(TTF_2)^{\bullet+}$ dimer is reflected in a 2.6 kcal mol^{-1} stabilization of the TTF-in coconformation of $\mathbf{6}_{in}^{9+}$. Further oxidation to the 7^{10+} state results in stronger electrostatic repulsion, and the coconformation with two neutral DNP units inside the octacationic molecular square and two $TTF^{\bullet+}$ driven away from the square is more thermodynamically stable (Figure 11), as verified by the much larger (28.7 kcal mol^{-1}) energetic penalty of including two $TTF^{\bullet+}$ units, which do not exist as a stabilized radical dimer $(TTF^{\bullet+})_2$ within the square. The energetic penalty for the TTF-in coconformation $\mathbf{6}^{10+}$ is much smaller (11.5 kcal mol^{-1}) and accounts for the experimentally observed $(TTF^{\bullet+})_2$ radical-cation dimer.

2.8. Summary. We have researched the role of topology on the stabilization of TTF radical dimers in three isomers. A mechanistic study in solution of the topological isomers, namely, the molecular Solomon link and the ring-in-ring complex, reveals a distinctive topological influence on oxidation of the TTF units expressed by the decomplexation of the macrocycle from the organoplatinum square in the ring-in-ring complex. The stabilization of the mixed-valence $(TTF_2)^{\bullet+}$ dimer upon one-electron oxidation of the TTF units is observed within the molecular frameworks of the mechanical/constitutional isomers, while the formation of the radical cationic $(TTF^{\bullet+})_2$ dimer occurs only transiently in the molecular Solomon link compared with the [3]catenane where this dimer is stabilized. When we analyze the solid-state structures of the TTF dimers in MIMs, the environment that the TTF units experience in the context of their specific topologies assumes considerable importance. The more highly constrained environment imposed by the topology of the molecular Solomon link, in comparison to other topologies, such as that present in the [3]catenane, results in a relative distortion on the TTF units located in the former.

3. CONCLUSION

The importance of topological effects upon the different redox states of closely interacting tetrathiafulvane units in topological and mechanical/conformational isomers has been uncovered.

dx.doi.org/10.1021/ja504662a | J. Am. Chem. Soc. 2014, 136, 11011–11026

The mechanically interlocked frameworks of the [3]catenane and molecular Solomon link isomers, both prepared in one step under thermodynamic control using template-directed protocols, present the ideal molecular setting for investigating the topological and mechanical effects of the radical recognition properties of pairs of tetrathiafulvalene units. The arrangement of the two electron-rich tetrathiafulvalene units directs the assembly of an organoplatinum square and presides over the formation of those two mechanical conformational isomers. The distinctively different topologies of the mechanical bonds in the [3]catenane and molecular Solomon link is reflected in the extent to which control is exercised over the relative stabilities of the $(TTF_2)^{\bullet+}$ mixed-valence and $(TTF^{\bullet+})_2$ radical cationic dimers. The demonstration of topological modulation of radical recognition properties provides an experimental basis for tailoring electronic interactions. The topological constraints present in the molecular Solomon link introduce a high level of dynamic structural complexity over the geometrical changes that occur during electronic stimulation of the tetrathiafulvalene units. The slow *reptation* of a crown ether around an organoplatinum square in this particular example of chemical topology resembles the more complex redox-controlled folding of cysteine knot in proteins.[4] Nature's tendency to minimize empty space, while exploiting noncovalent bonding interactions, is exhibited in the molecular structures of this doubly interlocked [2]catenane. The ability to tailor the properties of unnatural products by controlling their topologies paves the way for the investigation of more complex processes at the molecular and supramolecular levels that have yet to be explored in chemistry.

■ ASSOCIATED CONTENT

Supporting Information

Detailed synthetic procedures and characterization (NMR and HRMS) data for all compounds, spectroscopic (NMR and UV/vis) and electrochemical (CV and chronocoulometry) studies for the [3]rotaxane **6**·8PF_6 and the molecular Solomon link **7**·8PF_6, computational analysis for **6**·8PF_6, **6**·7PF_6·2ClO_4, **7**·8PF_6, and **7**·7PF_6·2ClO_4, and X-ray crystallographic analysis data (CIF) for **6**·8PF_6, **6**·7PF_6·2ClO_4, **7**·8PF_6, **7**·7PF_6·2ClO_4, **10**·8PF_6, **11**·8PF_6, (**4**⊂**8**)·8PF_6. This material is available free of charge via the Internet at http://pubs.acs.org.

■ AUTHOR INFORMATION

Corresponding Author

stoddart@northwestern.edu

Notes

The authors declare no competing financial interest.

■ ACKNOWLEDGMENTS

We thank Professor Jean-Pierre Sauvage (University of Strasbourg, France) for fruitful discussions. This research is part (Project 32-949) of the Joint Center of Excellence in Integrated Nano-Systems (JCIN) at King Abdul-Aziz City for Science and Technology (KACST) and Northwestern University (NU). The authors thank both KACST and NU for their continued support of this research. M.F. was supported by the Non-Equilibrium Energy Research Center (NERC), which is an Energy Frontier Research Center (EFRC) funded by the U.S. Department of Energy, Office of Basic Energy Sciences (DOE-BES), under Award DESC0000989. T.K. acknowledges the Japan Society for the Promotion of Science (JSPS) for the granting of a postdoctoral fellowship to carry out research abroad. D.C. is funded by a National Science Foundation (NSF) Graduate Research Fellowship and also acknowledges additional support from a Ryan Fellowship awarded by the Northwestern University International Institute for Nanotechnology (IIN). W.G.L. and W.A.G. were partially supported by NSF-EFRI-1332411. M.R.W. and S.M.D. are supported by the U.S. NSF under Grant No. CHE-1266201. R.C. is funded by the Argonne-Northwestern Solar Energy Research (ANSER) Center, which is an Energy Frontier Research Center (EFRC) funded by the U.S. Department of Energy, Office of Basic Energy Sciences (DOE-BES), under Award DE-SC0001059 (EPR Spectroscopy).

■ REFERENCES

(1) Mansfield, M. L. *Nat. Struct. Biol.* **1994**, *1*, 213−214.

(2) (a) Blankenship, J. W.; Dawson, P. E. *Protein Sci.* **2007**, *16*, 1249−1256. (b) Yeates, T. O.; Norcross, T. S.; King, N. P. *Curr. Opin. Chem. Biol.* **2007**, *6*, 213−214. (c) Shakhnovich, E. *Nat. Mater.* **2011**, *10*, 84−86.

(3) (a) Taylor, W. R. *Nature* **2000**, *406*, 916−919. (b) Mallam, A. L.; Jackson, S. E. *Structure* **2007**, *15*, 111−122. (c) King, N. P.; Jacobitz, A. W.; Sawaya, M. R.; Goldschmidt, L.; Yeates, T. O. *Proc. Natl. Acad. Sci. U.S.A.* **2011**, *108*, 17610−17614.

(4) Daly, N. L.; Craik, D. J. *Curr. Opin. Chem. Biol.* **2011**, *15*, 362−368.

(5) Tait, P. G. *Trans. R. Soc. Edinburgh* **1884**, *32*, 327−342.

(6) Alexander, J. W.; Briggs, G. B. *Ann. Math.* **1926−1927**, *28*, 562−586.

(7) (a) Hoste, J.; Morwen, T. *Math. Intell.* **1998**, *20*, 33−48. (b) Epple, M. *Arch. Hist. Exact Sci.* **1998**, *52*, 297−392. (c) Mislow, K. *Top. Stereochem.* **1999**, *22*, 1−82.

(8) Frisch, H. L.; Wasserman, E. *J. Am. Chem. Soc.* **1961**, *83*, 3789−3795.

(9) Schill, G. *Catenanes, Rotaxanes and Knots*; Academic Press: New York, 1971.

(10) Sauvage, J.-P., Dietrich-Buchecker, C., Eds. *Molecular Catenanes, Rotaxanes and Knots: A Journey through the World of Molecular Topology*; John Wiley & Sons: Weinheim, Germany, 1999.

(11) (a) Mitchell, D. K.; Sauvage, J.-P. *Angew. Chem., Int. Ed. Engl.* **1988**, *27*, 930−931. (b) Breault, G. A.; Hunter, C. A.; Mayers, P. C. *Tetrahedron* **1999**, *55*, 5265−5293. (c) Siegel, J. S. *Science* **2004**, *304*, 1256−1258. (d) Amabilino, D. B.; Pérez-García, L. *Chem. Soc. Rev.* **2009**, *38*, 1562−1571. (e) Forgan, R. S.; Sauvage, J.-P.; Stoddart, J. F. *Chem. Rev.* **2011**, *111*, 5434−5464.

(12) Walba, D. M. *Tetrahedron* **1985**, *41*, 3161−3212.

(13) Metal templation: (a) Dietrich-Buchecker, C. O.; Sauvage, J.-P. *Chem. Rev.* **1987**, *87*, 795−810. (b) Fujita, M.; Ibukuro, H.; Hagihara, H.; Ogura, K. *Nature* **1994**, *367*, 720−723. (c) Leigh, D. A.; Lusby, P. J.; Teat, S. J.; Wilson, A. J.; Wong, J. K. Y. *Angew. Chem., Int. Ed.* **2001**, *40*, 1538−1543. (d) Dietrich-Buchecker, C. O.; Colasson, B. X.; Sauvage, J.-P. *Top. Curr. Chem.* **2005**, *249*, 261−283. (e) Goldup, S. M.; Leigh, D. A.; Long, T.; McGonigal, P. R.; Symes, M. D.; Wu, J. *J. Am. Chem. Soc.* **2009**, *131*, 15924−15929. (f) Prikhodóko, A. I.; Sauvage, J.-P. *J. Am. Chem. Soc.* **2009**, *131*, 6794−6807. (g) Beves, J. E.; Blight, B. A.; Campbell, C. J.; Leigh, D. A.; McBurney, R. T. *Angew. Chem., Int. Ed.* **2011**, *50*, 9260−9327. (h) Ayme, J.-F.; Baves, J. E.; Campbell, C. J.; Leigh, D. A. *Chem. Soc. Rev.* **2013**, *42*, 1700−1712.

(14) Donor−acceptor interactions: (a) Ashton, P. R.; Goodnow, T. T.; Kaifer, A. E.; Reddington, M. V.; Slawin, A. M. Z.; Spencer, N.; Stoddart, J. F.; Vicent, C.; Williams, D. J. *Angew. Chem., Int. Ed. Engl.* **1989**, *28*, 1396−1399. (b) Anelli, P.-L.; Spencer, N.; Stoddart, J. F. *J. Am. Chem. Soc.* **1991**, *113*, 5131−5133. (c) Anderson, S.; Anderson, H. L.; Sanders, J. K. M. *Acc. Chem. Res.* **1993**, *26*, 469−475. (d) Hamilton, D. G.; Davies, J. E.; Prodi, L.; Sanders, J. K. M. *Chem.—Eur. J.* **1998**, *4*, 608−620. (e) Hamilton, D. G.; Feeder, N.; Prodi, L.; Teat, S. J.; Clegg, W.; Sanders, J. K. M. *J. Am. Chem. Soc.* **1998**, *120*, 1096−1097.

(f) Kaiser, G.; Jarrosson, T.; Otto, S.; Ng, Y.-F.; Bond, A. D.; Sanders, J. K. M. *Angew. Chem., Int. Ed.* **2004**, *43*, 1959−1962. (g) Au-Yeung, H. Y.; Dan Pantoş, G.; Sanders, J. K. M. *J. Am. Chem. Soc.* **2009**, *131*, 16030−16032. (h) Cao, D.; Amelia, M.; Klivansky, L. M.; Koshkakaryan, G.; Khan, S. I.; Semeraro, M.; Silvi, S.; Venturi, M.; Credi, A.; Liu, Y. *J. Am. Chem. Soc.* **2010**, *132*, 1110−1122. (i) Bruns, C. J.; Li, J.; Frasconi, M.; Schneebeli, S. T.; Iehl, J.; Jacquot de Rouville, H.-P.; Stupp, S. I.; Voth, G. A.; Stoddart, J. F. *Angew. Chem., Int. Ed.* **2014**, *53*, 1953−1958.

(15) Hydrogen bonding: (a) Hunter, C. A. *J. Chem. Soc., Chem. Commun.* **1991**, 749−751. (b) Vögtle, F.; Meier, S.; Hoss, R. *Angew. Chem., Int. Ed. Engl.* **1992**, *31*, 1619−1622. (c) Hunter, C. A. *J. Am. Chem. Soc.* **1992**, *114*, 5303−5311. (d) Adams, H.; Carver, F. J.; Hunter, C. A. *J. Chem. Soc., Chem. Commun.* **1995**, 809−810. (e) Johnston, A. G.; Leigh, D. A.; Pritchard, R. J.; Deegan, M. D. *Angew. Chem., Int. Ed. Engl.* **1995**, *34*, 1209−1212. (f) Yamamoto, C.; Okamoto, Y.; Schmidt, T.; Jäger, R.; Vögtle, F. *J. Am. Chem. Soc.* **1997**, *119*, 10547−10548. (g) Lukin, O.; Kuboto, T.; Okamoto, Y.; Schelhase, F.; Yoneva, A.; Müller, W. M.; Müller, U.; Vögtle, F. *Angew. Chem., Int. Ed.* **2003**, *42*, 4542−4545. (h) Chatterjee, M. N.; Kay, E. R.; Leigh, D. A. *J. Am. Chem. Soc.* **2006**, *128*, 4058−4073. (i) Ahmed, R.; Altieri, A.; D'Souza, D. M.; Leigh, D. A.; Mullen, K. M.; Papmeyer, M.; Slawin, A. M. Z.; Wong, J. K. Y.; Woollins, J. D. *J. Am. Chem. Soc.* **2011**, *133*, 12304−12310.

(16) Solvophobic forces: (a) Harada, A.; Li, J.; Kamachi, M. *Nature* **1992**, *356*, 325−327. (b) Anderson, S.; Anderson, H. L. *Angew. Chem., Int. Ed. Engl.* **1996**, *35*, 1956−1959. (c) Craig, M. R.; Hutchings, M. G.; Claridge, T. D. W.; Anderson, H. L. *Angew. Chem., Int. Ed.* **2001**, *40*, 1071−1074. (d) Harada, A. *Acc. Chem. Res.* **2001**, *34*, 456−464. (e) Kim, K. *Chem. Soc. Rev.* **2002**, *31*, 96−107. (f) Murakami, H.; Kawabuchi, A.; Matsumoto, R.; Ido, T.; Nakashima, N. *J. Am. Chem. Soc.* **2005**, *127*, 15891−15899. (g) Qu, D.-H.; Wang, Q.-C.; Tian, H. *Angew. Chem., Int. Ed.* **2005**, *44*, 5296−5299. (h) Cheetham, A. G.; Hutchings, M. G.; Claridge, T. D. W.; Anderson, H. L. *Angew. Chem., Int. Ed.* **2006**, *45*, 1596−1599. (i) Ke, C.; Strutt, N. L.; Li, H.; Hou, X.; Hartlieb, K. J.; McGonigal, P. R.; Ma, Z.; Iehl, J.; Stern, C. L.; Cheng, C.; Zhu, Z.; Vermeulen, N. A.; Meade, T. J.; Botros, Y. Y.; Stoddart, J. F. *J. Am. Chem. Soc.* **2013**, *135*, 17019−17030.

(17) Anion coordination: (a) Hübner, G. M.; Gläser, J.; Seel, C.; Vögtle, F. *Angew. Chem., Int. Ed.* **1999**, *38*, 383−386. (b) Shukla, R.; Deetz, M. J.; Smith, B. D. *Chem. Commun.* **2000**, 2397−2398. (c) Wisner, J. A.; Beer, P. D.; Drew, M. G. B.; Sambrook, M. R. *J. Am. Chem. Soc.* **2002**, *124*, 12469−12476. (d) Evans, N. H.; Beer, P. D. *Chem.—Eur. J.* **2011**, *17*, 10542−10546. (e) Spence, G. T.; Beer, P. D. *Acc. Chem. Res.* **2013**, *46*, 571−586.

(18) Radical templation: (a) Li, H.; Fahrenbach, A. C.; Coskun, A.; Zhu, Z.; Barin, G.; Zhao, Y.-L.; Botros, Y. Y.; Sauvage, J.-P.; Stoddart, J. F. *Angew. Chem., Int. Ed.* **2011**, *50*, 6782−6788. (b) Li, H.; Zhu, Z.; Fahrenbach, A. C.; Savoie, B. M.; Ke, C.; Barnes, J. C.; Lei, J.; Zhao, Y.-L.; Lilley, L. M.; Marks, T. J.; Ratner, M. A.; Stoddart, J. F. *J. Am. Chem. Soc.* **2013**, *135*, 456−467. (c) Barnes, J. C.; Fahrenbach, A. C.; Cao, D.; Dyar, S. M.; Frasconi, M.; Giesener, M. A.; Benítez, D.; Tkatchouk, E.; Chernyashevskyy, O.; Shin, W. H.; Li, H.; Sampath, S.; Stern, C. L.; Sarjeant, A. A.; Hartlieb, K. J.; Liu, Z.; Carmieli, R.; Botros, Y. Y.; Choi, J. W.; Slawin, A. M. Z.; Ketterson, J. B.; Wasielewski, M. R.; Goddard, W. A., III; Stoddart, J. F. *Science* **2013**, *339*, 429−433.

(19) Stoddart, J. F. *Chem. Soc. Rev.* **2009**, *38*, 1802−1820.

(20) (a) Dietrich-Buchecker, C. O.; Sauvage, J.-P.; Kintzinger, J.-P. *Tetrahedron Lett.* **1983**, *24*, 5095−5098. (b) Dietrich-Buchecker, C. O.; Sauvage, J.-P.; Kern, J.-M. *J. Am. Chem. Soc.* **1984**, *106*, 3043−3045. (c) Ashton, P. R.; Brown, C. L.; Chrystal, E. J. T.; Goodnow, T.; Kaifer, A. E.; Parry, K. P.; Philp, D.; Slawin, A. M. Z.; Spencer, N.; Stoddart, J. F.; Williams, D. J. *J. Chem. Soc., Chem. Commun.* **1991**, *9*, 634−639. (d) Gunter, M. J.; Hockless, D. C. R.; Johnston, M. R.; Skelton, B. W.; White, A. H. *J. Am. Chem. Soc.* **1994**, *116*, 4810−4823. (e) Fujita, M.; Aoyagi, M.; Ibukuro, F.; Ogura, K.; Yamaguchi, K. *J. Am. Chem. Soc.* **1998**, *120*, 611−612. (f) Fujita, M. *Acc. Chem. Res.* **1999**, *32*, 53−61. (g) Hernández, J. V.; Kay, E. R.; Leigh, D. A. *Science* **2004**, *306*, 1532−1537. (h) Loren, J. C.; Gantzel, P.; Linden, A.; Siegel, J. S. *Org. Biomol. Chem.* **2005**, *3*, 3105−3116. (i) Nakatani, Y.; Furusho, Y.; Yashima, E. *Angew. Chem., Int. Ed.* **2010**, *49*, 5463−5467. (j) Zhu, Z.; Fahrenbach, A. C.; Li, H.; Barnes, J. C.; Liu, Z.; Dyar, S. M.; Zhang, H.; Lei, J.; Carmieli, R.; Sarjeant, A. A.; Stern, C. L.; Wasielewski, M. R.; Stoddart, J. F. *J. Am. Chem. Soc.* **2012**, *134*, 11709−11720. (k) Black, S. P.; Stefankiewicz, A. R.; Smulders, M. M.; Sattler, D.; Schalley, C. A.; Nitschke, J. R.; Sanders, J. K. M. *Angew. Chem., Int. Ed.* **2013**, *52*, 5749−5752. (l) Li, S.; Huang, J.; Cook, T. R.; Pollock, J. B.; Kim, H.; Chi, K. W.; Stang, P. J. *J. Am. Chem. Soc.* **2013**, *135*, 2084−2087.

(21) (a) Dietrich-Buchecker, C. O.; Sauvage, J.-P. *Angew. Chem., Int. Ed. Engl.* **1989**, *28*, 189−192. (b) Chambron, J.-C.; Dietrich-Buchecker, C. O.; Sauvage, J.-P. *Top. Curr. Chem.* **1993**, *165*, 131−162. (c) Ashton, P. R.; Matthews, O. A.; Menzer, S.; Raymo, F. M.; Spencer, N.; Stoddart, J. F.; Williams, D. J. *Leibigs Ann. Recl.* **1997**, 2485−2494. (d) Safarowsky, O.; Nieger, M.; Fröhlich, R.; Vögtle, F. *Angew. Chem., Int. Ed.* **2000**, *39*, 1616−1618. (e) Perret-Aebi, L.-M.; von Zelewsky, A.; Dietrich-Buchecker, C.; Sauvage, J.-P. *Angew. Chem., Int. Ed.* **2004**, *43*, 4482−4485. (f) Lukin, O.; Vögtle, F. *Angew. Chem., Int. Ed.* **2005**, *44*, 1456−1477. (g) Guo, J.; Mayers, P. C.; Breault, G. A.; Hunter, C. A. *Nat. Chem.* **2010**, *2*, 218−222. (h) Arias, K. I.; Zysman-Colman, E.; Loren, J. C.; Linden, A.; Siegel, J. S. *Chem. Commun.* **2011**, *47*, 9588−9590. (i) Gonnuswamy, N.; Cougnon, F. B. L.; Clough, J. M.; Dan Pantos, G.; Sanders, J. K. M. *Science* **2012**, *338*, 783−785.

(22) (a) Ayme, J. F.; Beves, J. E.; Leigh, D. A.; McBurney, R. T.; Rissanen, K.; Schultz, D. *Nat. Chem.* **2012**, *4*, 15−20. (b) Ayme, J. F.; Beves, J. E.; Leigh, D. A.; McBurney, R. T.; Rissanen, K.; Schultz, D. *J. Am. Chem. Soc.* **2012**, *134*, 9488−9497.

(23) (a) Nierengarten, J.-F.; Dietrich-Buchecker, C. O.; Sauvage, J.-P. *J. Am. Chem. Soc.* **1994**, *116*, 375−376. (b) Dietrich-Buchecker, C. O.; Sauvage, J.-P. *Chem. Commun.* **1999**, 615−616. (c) Ibukuro, F.; Fujita, M.; Yamaguchi, K.; Sauvage, J.-P. *J. Am. Chem. Soc.* **1999**, *121*, 11014−11015. (d) McArdle, C. P.; Vittal, J. J.; Puddephatt, R. *Angew. Chem., Int. Ed.* **2000**, *39*, 3819−3822. (e) Pentecost, C. D.; Chichak, K. S.; Peters, A. J.; Cave, G. W.; Cantrill, S. J.; Stoddart, J. F. *Angew. Chem., Int. Ed.* **2007**, *46*, 218−222. (f) Peinador, C.; Blanco, V.; Quintela, J. M. *J. Am. Chem. Soc.* **2009**, *131*, 920−921. (g) Beves, J. E.; Campbell, C. J.; Leigh, D. A.; Pritchard, R. G. *Angew. Chem., Int. Ed.* **2013**, *52*, 6464−6467.

(24) (a) Chichak, K. S.; Cantrill, S. J.; Pease, A. R.; Chiu, S.-H.; Cave, G. W. V.; Atwood, J. L.; Stoddart, J. F. *Science* **2004**, *304*, 1308−1312. (b) Meyer, C. D.; Forgan, R. S.; Chichak, K. S.; Peters, A. J.; Tangchaivang, N.; Cave, G. W. V.; Khan, S. I.; Cantrill, S. J.; Stoddart, J. F. *Chem.—Eur. J.* **2010**, *16*, 12570−12581.

(25) Chambron, J.-C.; Sauvage, J.-P. *New J. Chem.* **2013**, *37*, 49−57.

(26) (a) Saitta, A. M.; Soper, P. D.; Wasserman, E.; Klein, M. L. *Nature* **1999**, *399*, 46−48. (b) Tezuka, Y.; Oike, H. *J. Am. Chem. Soc.* **2001**, *123*, 11570−11576. (c) Yamamoto, T.; Tezuka, Y. *Polym. Chem.* **2011**, *2*, 1930−1941. (d) Rosa, A.; Orlandini, E.; Tubiana, L.; Micheletti, C. *Macromolecules* **2011**, *44*, 8668−8680.

(27) (a) Tkalec, U.; Ravnik, M.; Čopar, S.; Žumer, S.; Muševič, I. *Science* **2011**, *333*, 62−65. (b) Senyuk, B.; Liu, Q.; He, S.; Kamien, R. D.; Kusner, R. B.; Lubensky, T. C.; Smalyukh, I. I. *Nature* **2013**, *493*, 200−205. (c) Seč, D.; Copar, S.; Zumer, S. *Nat. Commun.* **2014**, *5*, 3057.

(28) (a) Nielsen, M. B.; Lomholt, C.; Becher, J. *Chem. Soc. Rev.* **2000**, *29*, 153−164. (b) Bendikov, M.; Wudl, F.; Perepichka, D. F. *Chem. Rev.* **2004**, *104*, 4891−4945. (c) Yamada, J.-I., Sugimoto, T., Eds. *TTF Chemistry: Fundamentals and Applications of Tetrathiafulvalene*; Kodansha Springer: Berlin, 2004. (d) Jeppesen, J. O.; Nielsen, M. B.; Becher, J. *Chem. Rev.* **2004**, *104*, 5115−5131. (e) Fukuzumi, S.; Ohkubo, K.; D'Souza, F.; Sessler, J. L. *Chem. Commun.* **2012**, *48*, 9801−9815.

(29) (a) Wudl, F.; Wobschal, D.; Hufnagel, E. J. *J. Am. Chem. Soc.* **1972**, *94*, 670−672. (b) Ferraris, J.; Cowan, D. O.; Walatka, V.; Perlstein, J. H. *J. Am. Chem. Soc.* **1973**, *95*, 948−949. (c) Giffard, M.; Alonso, P.; Garín, J.; Gorgues, A.; Nguyen, T. P.; Richomme, P.;

Robert, A.; Roncali, J.; Uriel, S. *Adv. Mater.* **1994**, *6*, 298−300. (d) Collier, C. P.; Mattersteig, G.; Wong, E. W.; Luo, Y.; Beverly, K.; Sampaio, J.; Raymo, F. M.; Stoddart, J. F.; Heath, J. R. *Science* **2000**, *289*, 1172−1175. (e) Kwang-Fu Shen, C.; Duong, H. M.; Sonmez, G.; Wudl, F. *J. Am. Chem. Soc.* **2003**, *125*, 16206−16207. (f) Martín, N.; Sánchez, L.; Herranz, M. A.; Illescas, B.; Guldi, D. G. *Acc. Chem. Res.* **2007**, *40*, 1015−1024. (g) Ratera, I.; Veciana, A. *J. Chem. Soc. Rev.* **2012**, *41*, 303−349. (h) Pop, F.; Auban-Senzier, P.; Frąckowiak, A.; Ptaszyński, K.; Olejniczak, I.; Wallis, J. D.; Canadell, E.; Avarvari, N. *J. Am. Chem. Soc.* **2013**, *135*, 17176−17186.

(30) (a) Asakawa, M.; Ashton, P. R.; Balzani, V.; Credi, A.; Hamers, C.; Mattersteig, G.; Montalti, M.; Shipway, A. N.; Spencer, N.; Stoddart, J. F.; Tolley, M. S.; Venturi, M.; White, A. J. P.; Williams, D. J. *Angew. Chem., Int. Ed.* **1998**, *37*, 333−337. (b) Nielsen, K. A.; Cho, W. S.; Lyskawa, J.; Levillain, E.; Lynch, V. M.; Sessler, J. L.; Jeppesen, J. O. *J. Am. Chem. Soc.* **2006**, *128*, 2444−2451. (c) Spruell, J. M.; Paxton, W. F.; Olsen, J.-C.; Benítez, D.; Tkatchouk, E.; Stern, C. L.; Trabolsi, A.; Friedman, D. C.; Goddard, W. A., III; Stoddart, J. F. *J. Am. Chem. Soc.* **2009**, *131*, 115711−11580. (d) Canevet, D.; Sallé, M.; Zhang, G.; Zhang, D.; Zhu, D. *Chem. Commun.* **2009**, 2245−2269. (e) Fahrenbach, A. C.; Bruns, C. J.; Cao, D.; Stoddart, J. F. *Acc. Chem. Res.* **2012**, *45*, 1581−1592. (f) Bill, N. L.; Ishida, M.; Bähring, S.; Lim, J. M.; Lee, S.; Davis, C. M.; Lynch, V. M.; Nielsen, K. A.; Jeppesen, J. O.; Ohkubo, K.; Fukuzumi, S.; Kim, D.; Sessler, J. L. *J. Am. Chem. Soc.* **2013**, *135*, 10852−10862.

(31) Coskun, A.; Banaszak, M.; Astumian, R. D.; Stoddart, J. F.; Grzybowski, B. A. *Chem. Soc. Rev.* **2012**, *41*, 19−30.

(32) (a) Christensen, C. A.; Goldenberg, L. M.; Bryce, M. R.; Becher, J. *Chem. Commun.* **1998**, 509−510. (b) Ziganshina, A. Y.; Ko, Y. H.; Jeona, W. S.; Kim, K. *Chem. Commun.* **2004**, 806−807. (c) Yoshizawa, M.; Kumazawa, K.; Fujita, M. *J. Am. Chem. Soc.* **2005**, *127*, 13456−13457. (d) Rosokha, S. V.; Kochi, J. K. *J. Am. Chem. Soc.* **2007**, *129*, 828−838. (e) Aprahamian, I.; Olsen, J.-C.; Trabolsi, A.; Stoddart, J. F. *Chem.—Eur. J.* **2008**, *14*, 3889−3895. (f) Saad, A.; Barrière, F.; Levillain, E.; Vanthuyne, N.; Jeannin, O.; Fourmigué, M. *Chem.—Eur. J.* **2010**, *16*, 8020−8028. (g) Guasch, J.; Grisanti, L.; Souto, M.; Lloveras, V.; Vidal-Gancedo, J.; Ratera, I.; Painelli, A.; Rovira, C.; Veciana, J. *J. Am. Chem. Soc.* **2013**, *135*, 6958−6967. (h) Lipnická, Š.; Bělohradský, M.; Kolivoška, V.; Pospíšil, L.; Hromadová, M.; Pohl, R.; Chocholoušová, J. V.; Vacek, J.; Fiedler, J.; Stará, I. G.; Starý, I. *Chem.—Eur. J.* **2013**, *19*, 6108−6121.

(33) (a) Spruell, J. M.; Coskun, A.; Friedman, D. C.; Forgan, R. S.; Sarjeant, A. A.; Trabolsi, A.; Fahrenbach, A. C.; Barin, G.; Paxton, W. F.; Dey, S. K.; Olson, M. A.; Benítez, D.; Tkatchouk, E.; Colvin, M. T.; Carmielli, R.; Caldwell, S. T.; Rosair, G. M.; Gunatilaka Hewage, S.; Duclairoir, F.; Seymour, J. L.; Slawin, A. M. Z.; Goddard, W. A., III; Wasielewski, M. R.; Cooke, G.; Stoddart, J. F. *Nat. Chem.* **2010**, *2*, 870−879. (b) Coskun, A.; Spruell, J. M.; Barin, G.; Fahrenbach, A. C.; Forgan, R. S.; Colvin, M. T.; Carmieli, R.; Benítez, D.; Tkatchouk, E.; Friedman, D. C.; Sarjeant, A. A.; Wasielewski, M. R.; Goddard, W. A., III; Stoddart, J. F. *J. Am. Chem. Soc.* **2011**, *133*, 4538−4547.

(34) The term "*reptation*", from the Latin reptare (to creep), refers to how snakes crawl along a surface, slithering through one another. "*Reptation*" is used to rationalize the snake-like thermal motion of interwined and entangled long chain polymers, divided conceptually into sections known as reptons, which form the basis for the restricted motion. See: (a) De Gennes, P. G. *J. Chem. Phys.* **1971**, *55*, 572−579. (b) Barkema, G. T.; Panja, D.; Van Leeuwen, J. M. J. *J. Chem. Phys.* **2011**, *134*, 154901−154908. The term "*molecular reptation*" was introduced into the field of chemical topology to describe the dynamics of a molecular trefoil knot undergoing slow conformational changes. See: Dietrich-Buchecker, C. O.; Sauvage, J. P.; Kintzinger, J. P.; Maltese, P. *New J. Chem.* **1992**, *16*, 931−942.

(35) Since the [3]catenane $\mathbf{6}^{8+}$, the molecular Solomon link $\mathbf{7}^{8+}$, and the ring-in-ring complex $\mathbf{4}\subset\mathbf{8}^{8+}$ are individual chemical species with identical molecular formula ($C_{114}H_{140}O_{20}N_{12}S_8Pt_2$), we can classify them as isomers. For chemical isomer enumeration, see: Rouvray, D. H. *Chem. Soc. Rev.* **1974**, *3*, 355−372.

(36) Since the [3]catenane $\mathbf{6}^{8+}$ and the molecular Solomon link $\mathbf{7}^{8+}$ differ from each other in terms of their mechanically interlocked connectivity as well as the order of the attachment of their atoms, we use the term mechanical/constitutional isomers to describe the relationship between these two compounds.

(37) The [3]catenane $\mathbf{6}^{8+}$ and the ring-in-ring complex $\mathbf{4}\subset\mathbf{8}^{8+}$ can be considered to be constitutional isomers, since they differ most significantly in their constitutions and connectivity of their matrices, despite the [3]catenane having a mechanically interlocked structure, while the ring-in-ring complex is a supramolecular species composed of two rings.

(38) The molecular Solomon link $\mathbf{7}^{8+}$ and the ring-in-ring complex $\mathbf{4}\subset\mathbf{8}^{8+}$ are topological nontrivial isomers. They display the same chemical bond connectivity, but they cannot be interconverted by any deformative action in three-dimensional space without encountering crossing points or nodes. See refs 8, 9, and 12.

(39) (a) Fujita, M.; Ibukuro, F.; Yamaguchi, K.; Ogura, K. *J. Am. Chem. Soc.* **1995**, *117*, 4175−4176. (b) Stang, P. J.; Chen, K.; Arif, A. M. *J. Am. Chem. Soc.* **1995**, *117*, 8793−8797. (c) Park, K.-M.; Kim, S.-Y.; Heo, J.; Whang, D.; Sakamoto, S.; Yamaguchi, K.; Kim, K. *J. Am. Chem. Soc.* **2002**, *124*, 2140. (d) Yamauchi, Y.; Yoshizawa, M.; Fujita, M. *J. Am. Chem. Soc.* **2008**, *130*, 5832−5833. (e) Northrop, B. H.; Zheng, Y. R.; Chi, K. W.; Stang, P. J. *Acc. Chem. Res.* **2009**, *42*, 1554−1163. (f) Yan, X.; Li, S.; Cook, T. R.; Ji, X.; Yao, Y.; Pollock, J. B.; Shi, Y.; Yu, G.; Li, J.; Huang, F.; Stang, P. J. *J. Am. Chem. Soc.* **2013**, *135*, 14036−14039.

(40) (a) Blanco, V.; Chas, M.; Abella, D.; Peinador, C.; Quintela, J. M. *J. Am. Chem. Soc.* **2007**, *129*, 13978−13986. (b) Blanco, V.; García, M. D.; Peinador, C.; Quintela, J. M. *Chem. Sci.* **2011**, *2*, 2407−2416. (c) Alvariño, C.; Pía, E.; García, M. D.; Blanco, V.; Fernández, A.; Peinador, C.; Quintela, J. M. *Chem.—Eur. J.* **2013**, *19*, 15329−15335.

(41) Wang, C.; Cao, D.; Fahrenbach, A. C.; Grunder, S.; Dey, S. K.; Sarjeant, A. A.; Stoddart, J. F. *Chem. Commun.* **2012**, *48*, 9245−9247.

(42) Data were collected at 100 K on a Bruker Kappa APEX CCD diffractometer equipped with a Cu Kα microsource with Quazar optics. Crystallographic data for the structures reported in this article have been deposited with the Cambridge Crystallographic Data Center (CCDC) as supplementary publications and can be obtained free of charge via www.ccdc.cam.ac.uk/data_request/cif.

(43) Crystal data for $\mathbf{7}\cdot 8PF_6$. $[C_{114}H_{140}O_{20}N_{12}S_8Pt_2\cdot(PF_6)_8]\cdot(CH_3CN)_{13}$, M = 4338.49, monoclinic, space group $P2_1/n$ (no. 14); a = 20.9976(11), b = 33.2264(17), c = 26.4897(15) Å; β = 100.672(3)°; V = 18161.5(17) Å^3, T = 99.99 K, Z = 4, μ(Cu Kα) = 5.387 mm^{-1}. A total of 32608 reflections were collected, of which 32608 were unique. Final $wR(F_2)$ = 0.1454. CCDC no.: 952939.

(44) Crystal data for $\mathbf{10}\cdot 8PF_6$. $[C_{114}H_{140}O_{20}N_{12}S_8Pd_2\cdot(CF_3O_3S)_{2.73}\cdot(PF_6)_{5.27}]\cdot(C_2H_3N)_{10}$, M = 4049.14, triclinic, space group $P1$ (no. 2); a = 15.7952(2), b = 20.6341(4), c = 29.3750(4) Å; α = 87.9230(10)°, β = 86.8350(10)°, γ = 76.4070(10)°; V = 9288.9(2) Å^3, T = 99.99 K, Z = 2, μ(Cu Kα) = 4.065 mm^{-1}. A total of 209383 reflections were collected, of which 33341 were unique. Final $wR(F_2)$ = 0.2395. CCDC no.: 975035.

(45) Crystal data for $\mathbf{6}\cdot 8PF_6$. $[C_{114}H_{140}N_{12}O_{20}S_8Pt_2\cdot(PF_6)_8]\cdot(CH_3CN)_2$, M = 3886.90, monoclinic, space group $P2_1/n$ (no. 14); a = 35.6937(10), b = 12.3490(4), c = 39.6287(11) Å; β = 99.3191(19)°; V = 17237.1(9) Å^3, T = 100.05 K, Z = 4, μ(Cu Kα) = 5.586 mm^{-1}. A total of 46063 reflections were collected, of which 13568 were unique. Final $wR(F_2)$ = 0.3193. CCDC no.: 965478.

(46) Crystal data for $\mathbf{9}\cdot 8PF_6$. $[C_{114}H_{140}N_{12}O_{20}S_8Pd_2\cdot(PF_6)_8]$, M = 3627.41, monoclinic, space group $C2/c$ (no. 15); a = 35.8988(19), b = 12.3423(6), c = 39.878(2) Å; β = 100.002(4)°; V = 17400.5(16) Å^3, T = 99.99 K, Z = 4, μ(Cu Kα) = 4.221 mm^{-1}. A total of 24963 reflections were collected, of which 8228 were unique. Final $wR(F_2)$ = 0.3771. CCDC no.: 965480.

(47) Crystal data for $(\mathbf{4}\subset\mathbf{8})\cdot 8PF_6$. $[C_{114}H_{140}O_{20}N_{12}S_8Pt_2\cdot(PF_6)_8]$, M = 3804.79, monoclinic, space group $C2/c$ (no. 15); a = 37.143(5), b = 13.161(3), c = 34.426(5) Å; β = 93.675(10)°; V = 16794(5) Å^3, T = 100.01 K, Z = 4, μ(Cu Kα) = 5.716. A total of 48795 reflections were

collected, of which 14099 were unique (R_{int} = 0.0769). Final $wR(F_2)$ = 0.2244. CCDC no.: 952941.

(48) We have attempted to investigate the redox behavior of the tetrathiafulvalene units enclosed within the molecular framework of the [3]catenane $\mathbf{9}^{8+}$ and the molecular Solomon link $\mathbf{10}^{8+}$. We have observed, however, an irreversible redox process upon electrochemical oxidation and reduction of $\mathbf{9}^{8+}$ and $\mathbf{10}^{8+}$, indicating the opening of the labile Pd−N bond in the organopalladium squares upon oxidation of the TTF units as result of the severe electrostatic repulsions.

(49) Fahrenbach, A. C.; Bruns, C. J.; Li, H.; Trabolsi, A.; Coskun, A.; Stoddart, J. F. *Acc. Chem. Res.* **2014**, *47*, 482−493.

(50) The slow molecular tumbling of $TTF^{\bullet+}$ radical species within the organoplatinum square of $\mathbf{7}^{8+}$ is responsible for the anisotropy detected in the EPR spectra, an observation that is supported by a control experiment performed on $TTF^{\bullet+}$ radical species in a high viscosity solution. In this experiment, the rotation of the paramagnetic molecules slows yielding an asymmetric hyperfine splitting pattern. For examples of EPR spectra of paramagnetic molecules in the slow motion regime, obtained either by cooling or by increasing the viscosity of the solvent, see: (a) Weil, J. A. *J. Magn. Reson.* **1971**, *4*, 394−399. (b) Stoll, S.; Schweiger, A. *Chem. Phys. Lett.* **2003**, *380*, 464−470. (c) Kaupp, M., Bühl, M., Malkin, V. G., Eds. *Calculation of NMR and EPR Parameters*; Wiley-VCH: Weinheim, Germany, 2004.

(51) Crystal data for $\mathbf{7}\cdot 7PF_6\cdot 2ClO_4$. $[C_{114}H_{140}O_{20}N_{12}S_8Pt_2\cdot(PF_6)_7\cdot(ClO_4)_2]\cdot(CH_3CN)_9$, M = 4228.20, triclinic, space group $P\bar{1}$ (no. 2); a = 17.1706(8), b = 20.6416(10), c = 27.7781(14) Å; α = 104.377(2)°, β = 102.420(2)°, γ = 99.953(2)°; V = 9043.6(8) Å^3, T = 99.99 K, Z = 2, μ(Cu Kα) = 5.556 mm^{-1}. A total of 179427 reflections were collected, of which 32487 were unique (R_{int} = 0.0324). Final $wR(F_2)$ = 0.1617. CCDC no.: 952940.

(52) Crystal data for $\mathbf{6}\cdot 7PF_6\cdot 2ClO_4$. $[C_{114}H_{140}O_{20}N_{21}S_8Pt_2\cdot(PF_6)_7\cdot(ClO_4)_2]\cdot(CH_3CN)_8$, M = 4228.20, triclinic, space group $P\bar{1}$ (no. 2); a = 17.1706(8), b = 20.6416(10), c = 27.7781(14) Å; α = 104.377(2)°, β = 102.420(2)°, γ = 99.953(2)°; V = 9043.6(8) Å^3, T = 99.99 K, Z = 2, μ(Cu Kα) = 5.556 mm^{-1}. A total of 179427 reflections were collected, of which 32487 were unique (R_{int} = 0.0324). Final $wR(F_2)$ = 0.1617. CCDC no.: 952940.

(53) We have observed the presence of close [C−H···F] contacts, with an average distance of 2.42 Å, between the tetrathiafulvalene units and the surrounding PF_6^- counterions (see the Supporting Information), which may possibly contribute to the solid-state stabilization of the shared positive charge on the two tetrathiafulvalene units within the octacationic oraganoplatinum square despite the presence of Coulombic repulsions.

(54) (a) Zhao, Y.; Truhlar, D. G. *Acc. Chem. Res.* **2008**, *41*, 157−167. (b) Jaguar 7.6; Schrodinger, LLC: New York, 2009.

(55) We have demonstrated previously that DFT using the M06 suite of functions provides accurate structural and energetic prediction of mechanically interlocked molecules. See: Benítez, D.; Tkatchouk, E.; Yoon, I.; Stoddart, J. F.; Goddard, W. A., III. *J. Am. Chem. Soc.* **2008**, *130*, 14928−14929.